K. Kirov, F. Leuterer, G. Pereverzev, F. Ryter, W. Suttrop
and ASDEX Upgrade Team

**Electron Cyclotron Resonance Heating
in ASDEX Upgrade:
Calculation and Experimental Authentication
of the Power Deposition Profile**

Electron Cyclotron Resonance Heating
in ASDEX Upgrade:
Calculation and Experimental Authentication
of the Power Deposition Profile

K. Kirov, F. Leuterer, G. Pereverzev, F. Ryter, W. Suttrop
and ASDEX Upgrade Team

Max-Planck-Institut für Plasmaphysik

Contents

1 Introduction

Electron Cyclotron Resonance Heating (ECRH) has shown its importance in tokamak studies and its present usage substantially exceeds its heating and current drive application. Perturbative transport studies, Neoclassical Tearing Mode (NTM) stabilization, sawteeth tailoring, current profile control and formation of Internal Transport Barriers (ITB) by ctr- Electron Cyclotron Current Drive (ECCD) are examples employing ECRH and its advantage to allow narrow well localized power deposition [1]. All these scenarios in which ECRH is involved require a good knowledge of its power deposition, particularly in unstationary situations like sweeping of magnetic field B, steering of the launched beam or in very novel frequency tunable gyrotron applications. However ECRH power deposition is sensitive to many factors: magnetic field B and equilibrium, plasma density n and electron temperature T_e which are flux functions, and a variety of geometrical factors such as launching angles, launcher position and initial shape of the beam.

This complex dependence of ECRH power deposition on various contributions requires numerical treatment of the problem and for that reason different raytracing and beamtracing codes are developed and employed worldwide. A particular challenge from the experimental point of view is the determination of the ECRH power deposition profile and the comparison with the calculated one. Experimentally this can be achieved by measuring the electron temperature response to transient ECRH power [2, 3, 4, 5, 6, 7, 8, 9, 10, 11, 12]. The main difficulty in this case comes from the diffusive broadening of the temperature perturbations which often acts on a shorter time scale than the time resolution of the measurement. Especially if the ECRH power input is narrow and well localized, the non zero heat diffusivity will make the perturbed temperature profile broader so that it is difficult to recover the initial deposition profile.

In this paper we present global and local studies of the ECRH power deposition in ASDEX Upgrade. It is organized as follows. Section 2 briefly describes ASDEX Upgrade and its ECRH system. Section 3 presents results for beam paths and ECRH power deposition from beamtracing calculations for typical examples of EC beam launched perpendicularly and obliquely. In Section 4 some theoretical treatments of the problem and the following consequences are reported. The results from slab model approximation and numerical simulations with consequences for the experiment are presented there as well. The experimental results for the ECRH power deposition are given in Section 5. A summary is given in Section 6.

2 ASDEX Upgrade ECRH system and diagnostics

The ASDEX Upgrade ECRH system consists of four gyrotrons working at $140 GHz$. At the usual value of the magnetic field $|B_t| \approx 2.5T$ in ASDEX Upgrade, this corresponds to second harmonic X mode of the EC wave [13], which is launched into the plasma from the Low Field Side (LFS) of the torus equatorial midplane, Figure 1. All gyrotrons are able to deliver $P_{ECRH} \approx 0.5MW$ for $2s$, of which $\approx 0.4MW$ are launched into the plasma. At the end of each transmission line a steerable mirror allows launching of the focused beam in the desired poloidal and toroidal direction. The beams have a circular cross-section and a Gaussian power density profile with $1/e$ half width of $0.015m$ at the focus which is at about $1m$ from the launcher along the ray path. In the usual lower single null divertor discharges in ASDEX Upgrade the magnetic axis is above the midplane by $0.05m$ to $0.1m$ and is accessible when the beams are launched at poloidal angle $\theta \approx -10°$, Figure 1a. By further change of θ in the range $\pm 32°$ the EC absorption can be displaced vertically along the resonance layer, which can also be shifted radially by changing
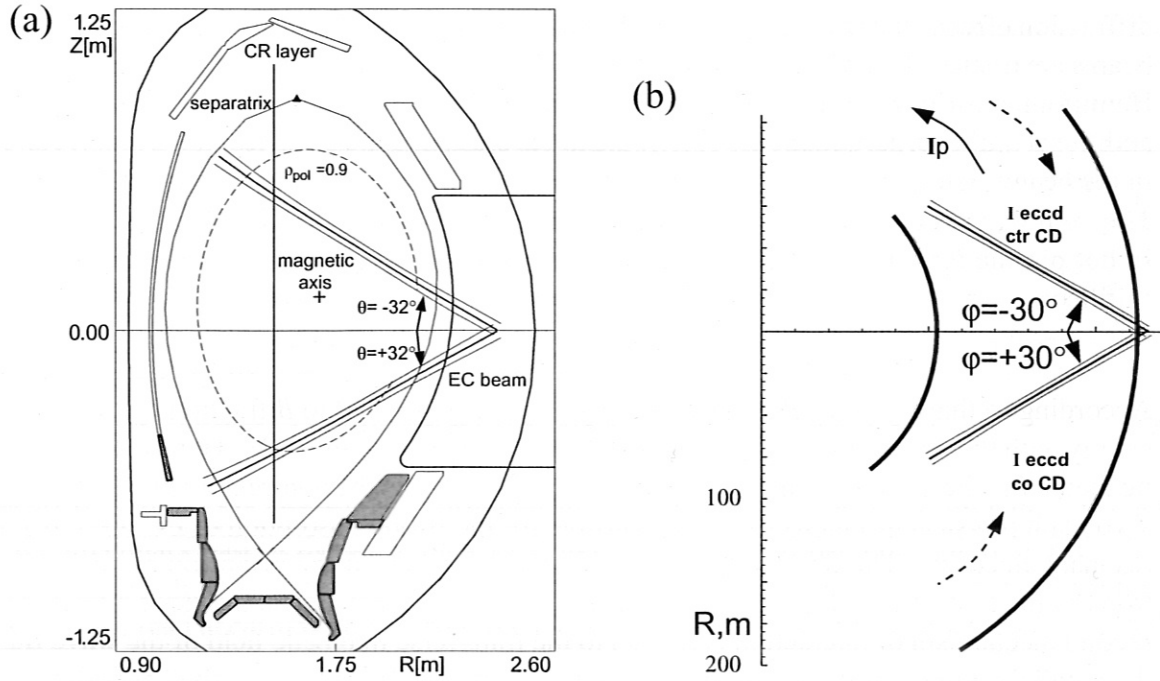
Figure 1: Poloidal cross-section (a) of the ASDEX Upgrade and toroidal midplane from the top (b) showing schematically the range of angles for the launched beams

the toroidal magnetic field B_t. By changing the toroidal launching angle φ in the range $\pm 30°$ the EC beam can be launched obliquely to produce co- or ctr- ECCD, Figure 1b.

The main diagnostic for electron temperature T_e measurements is the 60 channel ECE radiometer. It provides the electron temperature over the whole plasma cross-section with a time resolution of approximately $1/(30 kHz)$. The radial resolution of each channel is about $0.01 m$ [14]. The distance between the channels is $0.01 - 0.03 m$. The ion temperature T_i is measured by the Neutral Particle Analyzer diagnostic which yields T_i values at the magnetic axis and at about the half minor radius. The density profiles are obtained from the DCN interferometer, which measures the line averaged densities along 8 lines of sight. By combining the DCN interferometer data with the SOL density data, derived from the lithium beam diagnostic, reliable density profiles over the complete radial range are produced [15].

In ASDEX Upgrade two flux coordinates are defined and utilized: the normalized toroidal flux radius ρ and the normalized poloidal flux radius ρ_{pol}. In our study subscript "0" to these coordinates will indicate the position of the ECRH deposition center.

3   EC wave propagation, EC absorption and ECRH power deposition

The propagation properties of EC wave are not strongly affected by the kinetic effects in plasma and thus the wave propagation can be described in the approximation of cold plasma dispersion relation. Two approaches are usually used for drawing the path of the EC beam in the plasma: raytracing and beamtracing. In the raytracing approach the EC beam is divided into many rays and the solution of equations in Hamiltonian form yields the trajectory for each ray. Since the geometrical optics theory is applied here and the rays are considered separately, neglecting the

diffraction effects, the raytracing approach is not very precise when very focused or collimated beams are treated. In the beamtracing approach the beam is considered as a whole. Equations in Hamiltonian form are utilized again for calculation of the trajectory of the central ray, but now additional higher order equations, describing the evolution of the beam front, are involved. Thus in the beamtracing approach the diffraction effects are more accurately accounted for.

The cold plasma dispersion relation could not be employed in the vicinity of EC resonance. In hot plasma X and O modes have resonance when the wave particle resonance condition is fulfilled:

$$\omega - l\omega_c/\gamma = k_{\parallel}v_{\parallel}, \qquad \gamma = 1/\sqrt{1 - v^2/c^2}, \tag{1}$$

According to that equation electrons with velocity v and parallel to B fraction $v_{\parallel}$ can exchange energy with the wave with frequency ω and parallel to B wave number $k_{\parallel}$. Here γ is the relativistic factor, l is the EC wave harmonic number, $\omega_c = eB/m_0c$ is the non-relativistic EC frequency. Two main physical mechanisms are responsible for the strong absorption of EC wave from the resonant electrons. The first one is the resonant acceleration of the cyclotron rotation of electrons by the circularly polarized electric field of the wave E_w rotating in the same direction. The second mechanism of interaction is related to the transverse magnetic field of the wave B_w and the parallel component of the electron velocity $v_{\parallel}$. In both cases the absorbed energy from the wave increases mainly the perpendicular energy component of the resonant electrons. The absorption of the EC beam propagating in the plasma starts when a part of its phase front satisfies (1).

A good illustrative way of investigating the EC absorption in the plasma is the plot of the resonant curves, Figure 2, which are solutions of (1) in the velocity space $(v_{\perp}, v_{\parallel})$. Two different

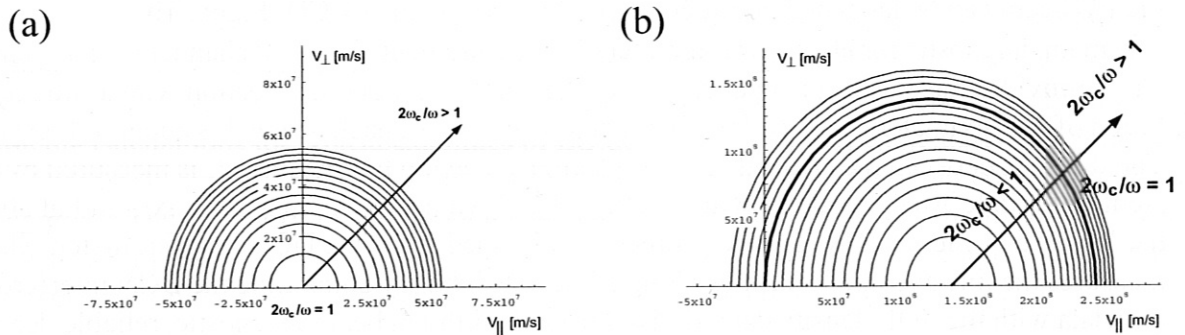(a)   (b)

Figure 2: EC resonant curves in velocity space at perpendicular launching (a) and in case of oblique launching (b)

cases of 2nd harmonic X mode EC wave, launched from LFS in $\approx 5keV$ low density plasma are shown in Figure 2. When launching perpendicularly, $k_{\parallel} = 0$, Doppler shift is equal to zero, and wave particle resonance condition transforms to $\omega = 2\omega_c/\gamma$. The resonant curves in velocity space are shown in Figure 2a. Due to relativistic factor the wave absorption is shifted to the HFS from the classical resonance layer. The resonant curves are symmetric circles, the wave absorption starts at the point $(v_{\perp} \cong 0, v_{\parallel} \cong 0)$, i.e. with slow electrons for which $v < v_{th}$ and mainly thermal electrons absorb energy from the wave.

In case of oblique launching of EC wave, $k_{\parallel} \neq 0$, the involved by the Doppler shift asymmetry in the wave-particle resonance condition causes shift of the resonant curves in velocity space, Figure 2b. The resonant curves are elongated ellipses. Concerning the ratio $2\omega_c/\omega$ there are two regions in resonant curves picture: up-shifted absorption when the frequency of the launched

wave is higher than the cyclotron frequency, and down-shifted absorption when ω is lower than $2\omega_c$, which is easier to be achieved when launching from HFS, when the beam propagation corresponds to a movement in direction to the center of the resonant curves. When launching from LFS, i.e. moving in opposite direction in the the resonant curves picture with the wave propagation, mainly up-shifted absorption takes place. Due to the Doppler shift and involved asymmetry, electrons with certain $v_\parallel$ are preferably heated and that is underlying in ECCD generation. Absorption in this case starts with high energy electrons but with further propagation of the wave, both thermal and super-thermal electrons can absorb energy from the wave.

In the linear theory the fraction of EC wave power absorbed from the resonant electrons in fusion plasma is given by:

$$P_{abs}/P_0 = 1 - e^{-\int \alpha ds} \tag{2}$$

where $\alpha = 2k''$ is the absorption coefficient and the integral is over the beam path s. Here k'' is the imaginary part of the wave number k and can be derived from the solution of the local dispersion relation accounting for the kinetic effects in hot plasma. The absorption profile is then determined according to (2) from the local values of the absorption coefficient α and the geometry of the beam in the resonant region.

In fusion plasma more important quantity is the density of the deposited ECRH power $p_{ECRH}(\rho)$ which is derived from the absorbed power after normalizing it to the volume factor and mapping onto the flux surfaces. The Gaussian cross section of the EC beam justifies, in most cases [1], the approximation $p_{ECRH}(\rho)$ with a Gaussian curve, determined by the center of the deposition ρ_0 and the width of the deposition profile w_0.

The ECRH deposition profile depends on the self-location of three surfaces: the classical resonance layer, the beam front and the flux surfaces. The narrowest ECRH deposition profile in principle can be obtained when these three surfaces nearly coincide. In all other cases $p_{ECRH}(\rho)$ strongly depends on the geometry of the problem and its determination requires raytracing or beamtracing calculations.

4   Calculations of ECRH power deposition with TORBEAM

The EC power deposition for ASDEX Upgrade shots is calculated by the TORBEAM code [16, 17]. It implements beamtracing technique [16, 18] for drawing the propagation of the EC beam with Gaussian cross section in cold plasma. TORBEAM takes the full set of experimental conditions for a given shot including the necessary data from magnetics and essential kinetic profiles. A description of the utilized interface xbt is given in Appendix A. The beam is described in terms of the central ray trajectory, the evolution of the wave front and the width of the field profile. Wave damping is calculated on the central ray employing a numerical approach [19] which calculates the imaginary part of the wave vector k'' adopting a weakly relativistic approximation for the dielectric tensor and the absorption profile is determined according to (2). For the calculation of the deposited ECRH power density $p_{ECRH}(\rho)$ the absorption profile is mapped onto the flux surfaces. In this definition of $p_{ECRH}(\rho)$ one assumes instantaneous distribution of the absorbed heat over the flux surface and does not take into account the perpendicular diffusion during the finite time needed for this.

---

[1] Rare exceptions are for example the cases when EC absorption is localized quite on-axis or in the region where the beam front is tangential to the flux surfaces

4.1 Perpendicular launching of the beam, $\varphi = 0°$

In case of perpendicular launching of the beam into the plasma the EC wave absorption always starts on the High Field Side (HFS) of the classical resonance layer. For a magnetic field at the magnetic axis $B_t \approx -2.5T$ the deposition can be located close to the plasma center for a value of $\theta \approx -10°$ for which the beam goes almost through the magnetic axis, case 1 in Figure 3a. Deviations from that angle, for instance $\theta = -20°$, shift the deposition towards the plasma edge.
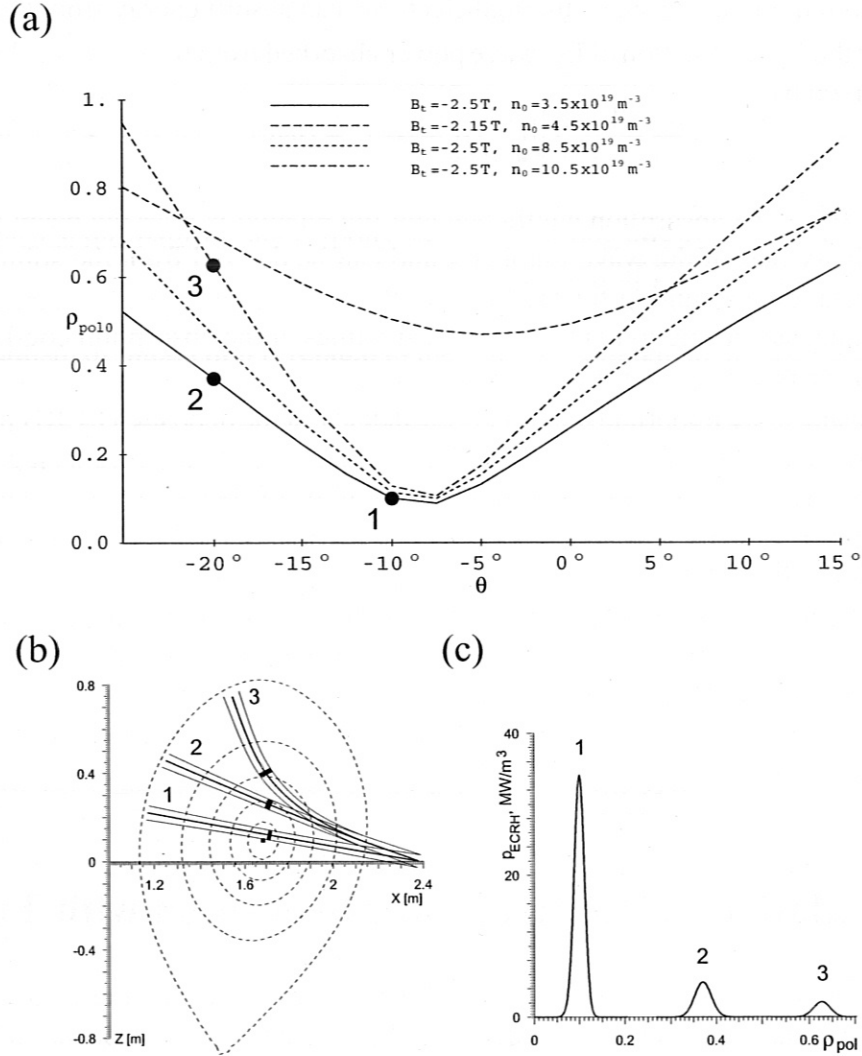

Figure 3: Poloidal sweep of the ECRH deposition center for $\varphi = 0°$ at different magnetic fields and densities (a), the beam paths (b) and the corresponding deposition profiles (c) for the selected three cases. At $B_t \approx -2.5T$ the ECRH deposition can be localized near the magnetic axis for $\theta \approx -10°$, case 1, and deviation of the beam from that launching angle shifts the deposition towards the plasma edge, cases 2 and 3. At higher density, case 3, due to the refraction of the beam the ECRH deposition shifts closer to the plasma edge.

At low density $n < 3 \times 10^{19} m^{-3}$ the plasma has little influence on the beam propagation which occurs nearly along a straight line, ray 2 in Figure 3b. At higher density the refraction of the beam becomes important, as shown by case 3 in Figure 3a. Note that in the case $\theta \approx -10°$ the density has little influence on the beam propagation.

In principle the ECRH deposition profile $p_{ECRH}(\rho)$ is determined by the beam width and by the

7

absorption along the propagation and the more dominant is the former contribution the broader $p_{ECRH}(\rho)$ will be observed. As an illustration of the case when the beam width does not influence $p_{ECRH}(\rho)$ we refer to Figure 4 case 1 (or case A) where the absorption is shifted to the HFS(LFS) by lower(higher) magnetic field and the beam front is tangential to the flux surfaces. In this case the deposition profile is very narrow because it is determined by the strong imaginary part of the wave vector, rather than by the beam width. At $B_t \approx -2.5T$ the ECRH deposition profile is always influenced by the beam width even in the case of on-axis deposition, Figure 3c, and thus it is impossible to gain very narrow deposition profile in this case. In spite of this $p_{ECRH}(\rho)$ remains sufficiently narrow and satisfies the requirements for well localized deposition.

4.2   Oblique launching of the beam, $\varphi \neq 0°$

In the case of variable oblique launching at fixed value of the poloidal launching angle θ, the EC wave absorption is mainly in the up-shifted region. Here, due to the Doppler shift, the absorption starts already at the LFS of the classical resonance layer. When the poloidal angle is

(a)

(b)

(c)

Figure 4: Toroidal sweep of the ECRH deposition center for $\theta = -10°$ at two different magnetic fields and low density $n < 4 \times 10^{19} m^{-3}$ (a), the beam paths (b) and the corresponding deposition profiles (c) for the selected six cases. The absorption always shifts to the LFS with increasing φ but at $|B_t| > 2.5T$ that corresponds to shift of the ECRH deposition towards the edge, sequence A, B, C, while at $|B_t| < 2.5T$ the ECRH deposition approaches the magnetic axis, sequence 1, 2, 3.

fixed such that the beam propagates through the center, i.e. $\theta \approx -10°$ and the toroidal angle φ only is changed, the deposition is shifted with φ either towards or away from the magnetic axis depending on the magnetic field B_t, Figure 4. At $|B_t| < 2.5T$ when the classical resonance layer is on the HFS the absorption shifts to lower magnetic field with φ, i.e. in a flux surfaces co-ordinate system the deposition center approaches the magnetic axis, Figure 4 points 1, 2, 3. In the opposite case when $|B_t| > 2.5T$ the absorption is on the LFS and the deposition center shifts to the edge with φ, Figure 4 points A, B, C. With increasing toroidal angle $k_{\parallel}$ increases and that leads to broadening of the absorption region and its shift to the LFS. The width of the deposition profile here is determined by the width of the absorption region and by the projection onto the flux surfaces.

The picture becomes more complicated when the poloidal angle θ is fixed so that the beam propagates far off-axis. In this case at larger magnetic field $|B_t| > 2.5T$, when the absorption is on the LFS, the same picture as in Figure 4 is observed: with increasing φ the absorption is displaced in direction of the LFS, i.e. the deposition center shifts to larger values of ρ_{pol}, Figure 5, $(B_t = -2.6T)$. However, at $|B_t| < 2.5T$ the absorption is on the HFS and a competition between

(a)

(b)

(c)
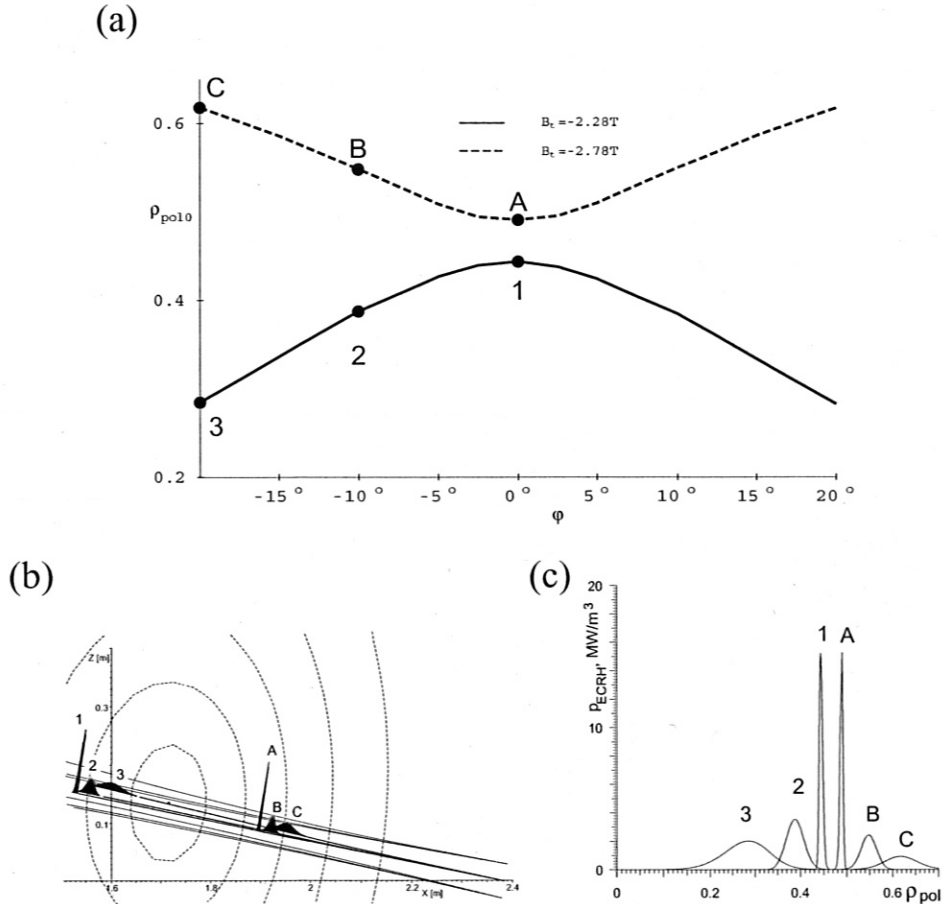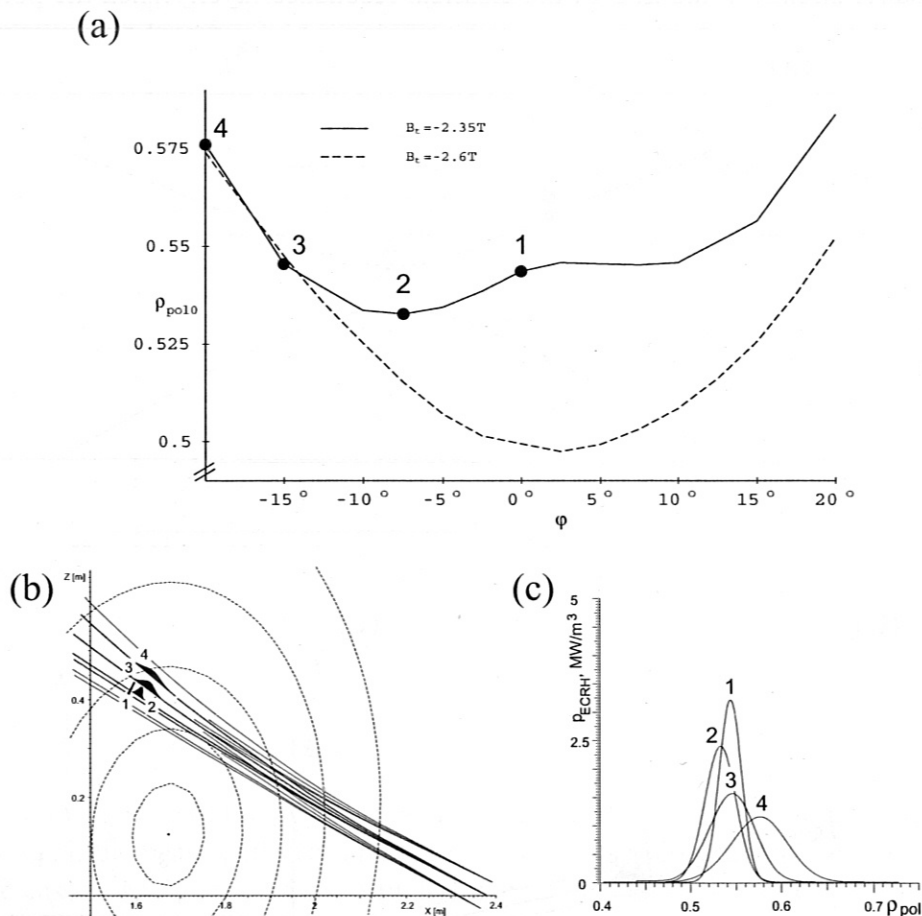

Figure 5: Toroidal scan of the ECRH deposition center for $\theta = -25°$ at two different magnetic and low density $n < 4 \times 10^{19} m^{-3}$ (a), the beam paths (b) and the corresponding deposition profiles (c) for the selected four cases

two effects is observed. At small angles φ the Doppler shift of the absorption determines the inward shift of the deposition center, case 2 in Figure 5. At larger values of φ because of the increased distance between the beam and the magnetic axis and hence larger apparent θ due to

increasing φ, the deposition shifts to the edge, case 4 in Figure 5. Here up shifted absorption again leads to broadening of the absorption and its shift to the LFS. The width of the deposition profile here is also determined by the width of the absorption region and by the projection onto the flux surfaces and increases with increasing the toroidal angle, Figure 5c.

5 Investigations of EC power deposition

The experimental investigation of the ECRH power deposition requires a time variation of the ECRH power, e.g. switch on/off or modulation. This is called the perturbative power in the following. In our study ECRH is the only explicit perturbative power, however in response to it the Ohmic input power and sinks may vary.

The time evolution of the electron temperature $T_e(r,t)$ obeys the energy transport equation:

$$\frac{3}{2}\frac{\partial}{\partial t}(n(r,t)T_e(r,t)) + \nabla\left(q_e(r,t) + \frac{5}{2}T_e(r,t)\Gamma_e(r,t)\right) =$$

$$= p_{ECRH}(r,t) + p_{in}(r,t) - p_{out}(r,t) + \Gamma_e(r,t)\frac{\nabla(n(r,t)T_e(r,t))}{n(r,t)} \tag{3}$$

In (3) $n(r,t)$ and $\Gamma_e(r,t)$ are the electron density and particle flux. In a general form the heat flux can be written as: $q_e(r,t) = -n(r,t)\chi_e(r,T_e,\nabla T_e)\nabla T_e(r,t) - n(r,t)U_e(r,T_e,\nabla T_e)T_e(r,t)$ where χ_e is the electron heat diffusivity and U_e is the convective velocity, both being functions of plasma parameters and their gradients. The ECRH power density is accounted for in $p_{ECRH}(r,t)$. The other input powers and the sinks are taken into account in $p_{in}(r,t)$ and $p_{out}(r,t)$, respectively. For the temperature perturbations $\delta T_e(r,t)$ — as a response to perturbative source $p_{ECRH}(r,t)$ — neglecting the possible density changes one derives the linearized expression [20, 21]:

$$n_0\frac{\partial}{\partial t}\delta T_e(r,t) + \frac{2}{3}\nabla\delta q_e(r,t) = -n_0 b\delta T_e(r,t) + \frac{2}{3}p_{ECRH}(r,t) \tag{4}$$

where $b = (2/3n_0)\ \partial(p_{out} - p_{in})/\partial T_e$ is the damping term which accounts for the balance between power inputs and losses, index 0 refers to the steady state. The perturbed heat flux can be presented [20] as: $\delta q_e(r,t) = -n_0\chi_{e,eff}(r,t)\nabla\delta T_e(r,t) - n_0 U_{e,eff}(r,t)\delta T_e(r,t)$ where $\chi_{e,eff}$ is the effective electron heat diffusivity, which characterises the transport of slightly perturbed temperature variations and $U_{e,eff}$ is the effective convective velocity. In the numerical simulations presented later we will use a purely diffusive transport model which describes $T_e(r,t)$ evolution without convection and $\chi_{e,eff}$ will be estimated according to [20, 21]:

$$\chi_{e,eff} = \chi_e + \frac{\partial\chi_e}{\partial\nabla T_e}\nabla T_e \tag{5}$$

The experiments in ASDEX Upgrade with off-axis ECRH does not yield any indication of convection [22] and the simulations [23] without convective velocity term $U_{e,eff}$ show good agreement with the observed experimental results. In the following calculations we will therefore not take into account the effective convective velocity.

The aim of this paper is the reconstruction of the ECRH power deposition profile from the local changes of the measured electron temperature in transient processes such as switching on/off or modulating the ECRH power. Therefore the equation (4) is employed for calculation of the temperature changes $dT_e(r,t)$ after switching on/off ECRH or the temperature oscillations $\tilde{T}_e(r,t)$ from modulated ECRH. The comparison of the experimental $dT_e(r,t)$ and $\tilde{T}_e(r,t)$ profiles to the solutions of equation (4) provides the experimental recovery of $p_{ECRH}(r,t)$.

5.1 Analytical solution for slab geometry

In order to understand the underlying physics it is instructive to simplify (4) and derive analytical solutions providing easily quantitative analysis of the problem and some important general conclusions. This is achieved assuming a homogeneous plasma slab, constant heat diffusivity $\chi_{e,eff}(x,t) = \chi_e = const$ and for the perturbed heat flux $\delta q_e(x,t) = -n_0\chi_e\partial\delta T_e(x,t)/\partial x$. One derives a linearized 1D heat diffusion equation that governs the perturbed electron temperature evolution $\delta T_e(x,t)$:

$$\frac{\partial\delta T_e(x,t)}{\partial t} = \frac{2}{3}\chi_e\frac{\partial^2\delta T_e(x,t)}{\partial x^2} - b\delta T_e(x,t) + \frac{2}{3n_0}p_{ECRH}(x,t) \qquad (6)$$

We also suppose that the damping term b and heat diffusivity χ_e are known. The EC heating power $p_{ECRH}(x,t)$ is **switched on** at $t = t_0$ and has Gaussian profile:

$$p_{ECRH}(x,t) = \frac{p_0}{\sqrt{\pi}w_0}e^{-\frac{(x-x_0)^2}{w_0^2}}H(t-t_0) \qquad (7)$$

determined by its width w_0, center of deposition x_0 and maximum $p_0/(\sqrt{\pi}w_0)$, where p_0 is the absorbed power per square meter and $H(t-t_0)$ is the Heaviside function. The temperature change $dT_e(x,t) = T_e(x,t) - T_e(x,t_0)$ after switching on ECRH is determined from the solution of (6) and in this case it is [12]:

$$dT_e(x,t) = ac\frac{e^{ab}}{\sqrt{ab}}\left\{\Psi\left(\sqrt{ab(1+t/a)},\sqrt{abg}\right) - \Psi\left(\sqrt{ab},\sqrt{abg}\right)\right\} \qquad (8)$$

where $a = 3w_0^2/8\chi_e$ is a characteristic time depending on the heat diffusivity χ_e and ECRH power deposition width w_0, $c = 2p_0/3n_0w_0$ and $g = (x-x_0)^2/w_0^2$. The function Ψ is defined as:

$$\Psi(\mu,v) = \frac{2}{\sqrt{\pi}}\int_0^\mu\exp\left(-\xi^2 - v^2/\xi^2\right)d\xi \qquad (9)$$

The time evolution of $dT_e(x,t)$ at different positions along the x-axis during $1ms$ after the ECRH switch on is shown in Figure 6. The parameters are: $t_0 = 0s$, $x_0 = 0m$, $p_0 = 15kW/m^2$, $b = 100s^{-1}$, $\chi_e = 1m^2/s$ and $n_0 = 2\times10^{19}m^{-3}$. The largest temperature increase dT_e is always at the center of the ECRH deposition. Inside the ECRH deposition region, i.e. $x \leqslant 0.02m$ in Figure 6a and $x \leqslant 0.04m$ Figure 6b, the temperature T_e rises instantaneously while outside this region the temperature rise is delayed. Thus the deposition center can always be determined from the maximum of dT_e, although the dT_e profile becomes broader, i.e. its width at $dT_{e,max}/e$ increases with time due to diffusion. Note that we define the width as $dT_{e,max}/e$, although the dT_e profile is not a Gaussian.

As can be seen from Figure 6a where $w_0 = 0.01m$ and $a = 40\mu s$, following the dashed line for $dT_e(x=0,t)/e$, at the time $t = 0.35ms$ after switching on ECRH the dT_e profile is twice broader, and after $1ms$ the dT_e profile is already three times broader. Further, due to the damping term b the temperature increase dT_e reaches saturation — in this case for $t \geqslant 0.02s$ — then the dT_e profile is nearly independent of the original deposition profile and that makes the determination of w_0 from the T_e response almost inaccessible. Indeed, taking the limit $t/a \to \infty$ in (8) we find that the dT_e profile becomes practically independent of $p_{ECRH}(x)$. Up to $t = a$ the temperature profile is very narrow and its width is rather close to w_0, Figure 6. For proper determination of w_0 one has to measure dT_e profile width within a time $t_{meas} < a$.
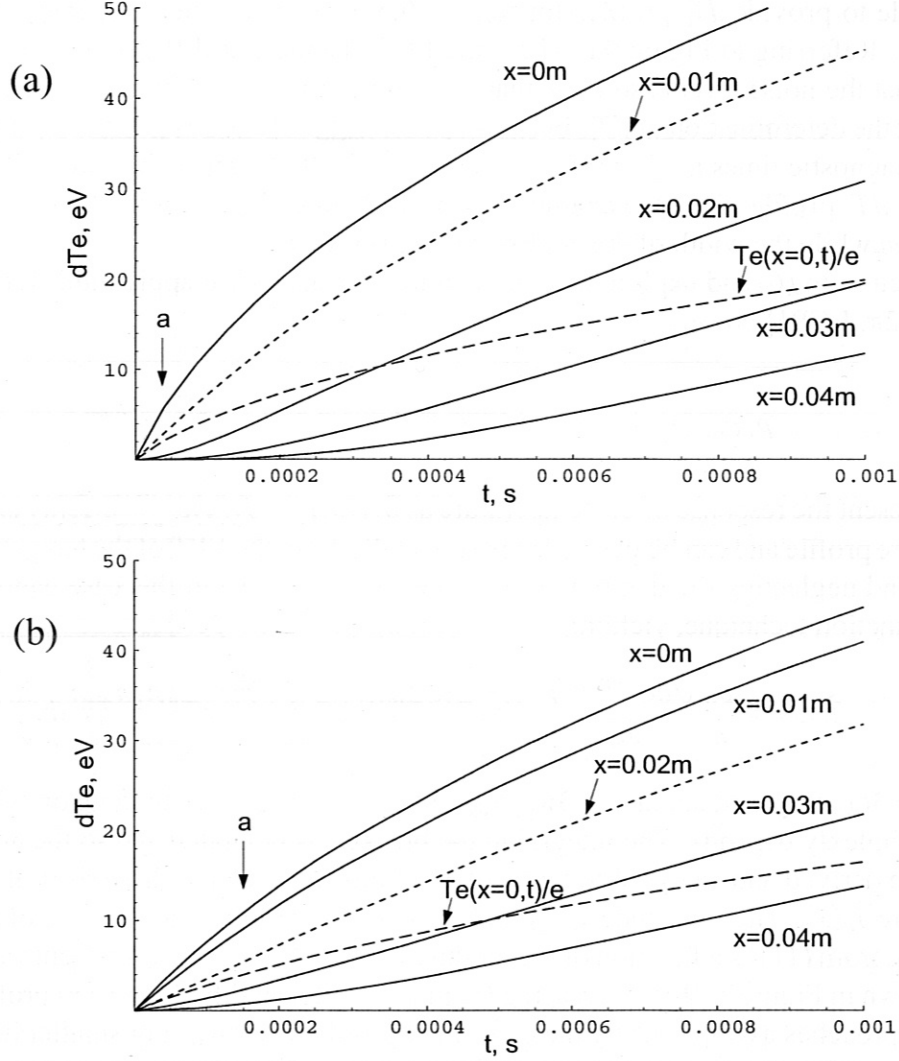
Figure 6: Electron temperature increase $dT_e(x,t) = T_e(x,t) - T_e(x,t_0)$ (solid curves) and $dT_e(x = 0,t)/e$ line (dash line) at different positions along x-axis after switch on ECRH with $w_0 = 0.01m$, $a = 40\mu s$ (a) and $w_0 = 0.02m$, $a = 160\mu s$ (b). The dotted lines correspond to the width of the ECRH deposition profile.

The absorption of the EC beam occurs on the HFS of the magnetic axis, and in ASDEX Upgrade with a spot size of about $50mm$ in diameter. The ECE measurements are done on the LFS, and therefore we rely on the distribution of the energy over the flux surfaces. For example if we heat at about half minor radius, the poloidal circumference of the flux surface in ASDEX Upgrade is about $2.5m$. Neglecting collisions and parallel electric field, one can estimate that electrons starting from the heated spot with a parallel velocity corresponding to $1keV$ will complete one turn around the torus in about $1\mu s$. In order to fill the flux surface with their energy they will need about 50 turns and that will take $t_{fill} \approx 50\mu s$ [12]. Then the requirement $t_{fill} < t_{meas} < a$ brings for typical values of the heat diffusivity $\chi_e \approx 1m^2/s$ the lower limit of the measurable profile width of about $0.01m$. In smaller devices this restriction may be much less severe. Even if we aim at measurement of broader ECRH deposition profiles, e.g. in the range $w_0 = 0.015 - 0.03m$ resulting in typical values of a between $\approx 85\mu s$ and $\approx 340\mu s$ so that the condition $a > t_{fill}$ is fulfilled, Figure 6b, we will face another limitation. It comes from the fact that the diagnostics

are not able to provide dT_e profiles for $t_{meas} < 0.5ms$ with sufficient accuracy and good time resolution. Referring to Figure 9a, where the ECE channels at different positions are shown, we note that the noise level is so large that T_e increase for about $300\mu s$ is comparable with the noises and the determination of dT_e and its slope for $t_{meas} < 0.5ms$ is practically impossible. For realistic diagnostic times $t_{meas} \gtrsim 0.5ms$, which is typically larger than a, we will then measure broadened dT_e profile: from the example shown in Figure 6b the width of dT_e after $0.5ms$ will be $\approx 0.03m$ while the width of the applied ECRH is $0.02m$.

Now we return to (6) and explore the temperature response if we apply **modulated**, frequency $f_m = \omega_m/2\pi$, ECRH power:

$$p_{ECRH}(x,t) = \tilde{p}_{ECRH}(x)e^{-i\omega_m t} = \frac{p_0}{\sqrt{\pi}w_0}e^{-\frac{(x-x_0)^2}{w_0^2}}e^{-i\omega_m t} \qquad (10)$$

We can present the response of the temperature as $\delta T_e(x,t) = \tilde{T}_e(x)e^{-i\omega_m t}$. $\tilde{T}_e(x)$ is the perturbed temperature profile and can be derived experimentally from the FFT of the temperature. Taking $x_0 = 0m$ and neglecting the damping term b the solution of (6) in this case can be derived by Green's function technique, yielding:

$$\tilde{T}_e(x) = \frac{p_0}{n}\frac{\sqrt{a}e^{-i\omega_m a}}{\sqrt{\omega_m}}\left(\sqrt{i\pi}e^{-2\sqrt{-ih x^2}} - 2\int_0^{\sqrt{\omega_m a}} e^{-hx^2/\tau^2 + i\tau^2}d\tau\right) \qquad (11)$$

where $h = 3\omega_m/8\chi_e$ and again $a = 3w_0^2/8\chi_e$ appears as characteristic time on which the $\tilde{T}_e(x)$ profile complexly depends. The integral in the brackets is tabulated and so the analytical solution can be derived and analysed in terms of amplitude profile and phase shift of the perturbed temperature $\tilde{T}_e(x)$. The amplitude $\tilde{T}_{emax}$ and the width, determined at $\tilde{T}_{emax}/e$, of the $\tilde{T}_e(x)$ profile derived from (11) as a function of the modulation frequency f_m for different values of χ_e and w_0 are shown in Figure 7. With increasing frequency f_m the width of the $\tilde{T}_e(x)$ profile is decreasing and approaches asymptotically the deposition profile width w_0. For smaller heat diffusivity or broader profile, the $\tilde{T}_e(x)$ profile tends faster to $p_{ECRH}(\rho)$. In all the cases of Figure 7 the amplitude $\tilde{T}_e(x = 0)$ decreases strongly with f_m, although weaker than $1/f_m$, and this is also a typical feature of the heat wave propagation. As a consequence the signal to noise ratio drops significantly at high f_m, limiting the upper useful frequency. If we assume for the realistic diagnostic time the time for which the temperature changes are well above the noise level, which in our case occurs at $t_{meas} \gtrsim 0.5ms$, then the useful frequency range in the modulation studies will be $1/\tau_e \ll f_m \lesssim 1/t_{meas}$, where τ_e is the electron energy confinement time.

5.2 ASTRA calculations

Based on a model for transport a direct solution of (3) is provided by numerical simulations. The advantage of such an approach is that toroidal geometry, experimental data and equilibrium as well as the other contributions in (3) are taken into account. Moreover the results depend on the assumed transport model.

In this study we used the ASTRA transport code [24], which is the main tool for transport studies in ASDEX Upgrade. It is a code for predictive and interpretative transport modelling and for processing experimental data. ASTRA incorporates a system of 2D equilibrium equation, 1D diffusion equations for densities and temperature of different plasma components and a variety of other modules describing additional heating, current drive and other non-diffusive processes in tokamak plasma. The transport coefficients can be specified in the code or given also externally. The Ohmic heating is determined assuming neoclassical conductivity, radiative power is
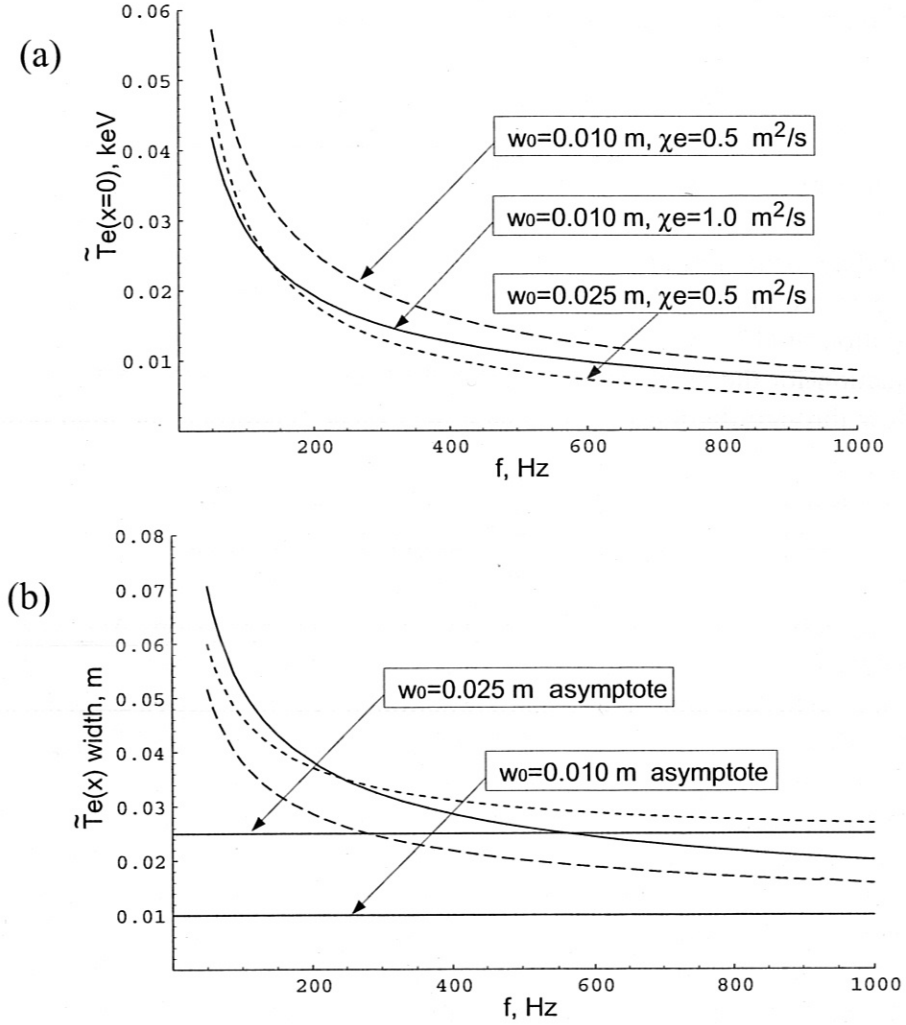
13

Figure 7: The amplitude $\tilde{T}_e(x=0)$ (a) and the width of $\tilde{T}_e(x)$ profile (b) for $\chi_e = 0.5m^2/s, w_0 = 0.01m$ (dash line), $\chi_e = 0.5m^2/s, w_0 = 0.025m$ (dotted line), $\chi_e = 1m^2/s, w_0 = 0.01m$ (solid line)

taken experimentally from bolometry. The electron heat flux is calculated with a heat diffusivity which is the sum of neoclassical and turbulent one based on the Weiland's model [25]. This model has been shown to simulate well ECRH heated discharges in ASDEX Upgrade [23]. In the modulated ECRH studies FFT is applied to T_e calculated by ASTRA, yielding the $\tilde{T}_e(\rho)$ and phase profiles.

Two different approaches are investigated with ASTRA. The **first** one assumes a known ECRH power deposition $p_{ECRH}(\rho)$, for instance from beamtracing. Then it can be accounted for in the electron energy balance and after choosing a suitable transport coefficients the $dT_e(\rho,t)$ evolution before and after switching ECRH or $\tilde{T}_e(\rho, \omega_m)$ profile in modulation studies can be derived and compared with the experiment. This approach is applied for determination of the deposition width w_0 in switch on/off and modulated ECRH experiments.

The **second** approach is based on the power balance scheme applied to (3) after providing it with the experimental values of T_e and n. The power balance yields the missing power input, i.e. in our case the total absorbed ECRH power, from the changes of the electron temperature $\Delta T_e(\rho,t) = T_e(\rho,t) - T_e(\rho,t_{0-})$ and the heat flow $\Delta q_e = q_e(\rho,t) - q_e(\rho,t_{0-})$ when ECRH power

14

is switched on at $t = t_0$ according to the linearized equation:

$$p_{ECRH}(\rho, t) = \frac{3}{2} n_0 \frac{\partial}{\partial t} \Delta T_e(\rho, t) + \nabla \Delta q_e(\rho, t) + \frac{3}{2} n_0 b \Delta T_e(\rho, t) \tag{12}$$

The direct determination of $p_{ECRH}(\rho, t)$ from (12) is possible only if $\Delta T_e(\rho, t)$ is measured immediately, for times $t_{meas} < a$, after turn on ECRH power. As it was shown from (8) and Figure 6 for realistic diagnostic times $t_{meas} > a$ the second term on the RHS in (12) becomes important in the $\Delta T_e(\rho, t)$ evolution and the diffusive broadening of the $\Delta T_e(\rho)$ profile is large. However, after integration of (12) over the plasma volume V_s enclosed by the separatrix we can reduce it to an equation for the changes of the total electron energy content $\Delta W_e = \int_{V_s} 3/2 n_0 \Delta T_e dV$, the heat flow through the plasma boundary $\Delta Q_e = \oint_{S_s} \Delta q_e dS$ and the total power of sources $\Delta P_{in} = \int_{V_s} \Delta p_{in} dV$ and sinks $\Delta P_{out} = \int_{V_s} \Delta p_{out} dV$ after switching on ECRH:

$$P_{ECRH} = \frac{d\Delta W_e}{dt} + \Delta Q_e - \Delta P_{in} + \Delta P_{out} \tag{13}$$

In (13) P_{ECRH} is the total absorbed ECRH power and the expressions $\Delta P_{in} = P_{in}(t) - P_{in}(t_{0-})$ and $\Delta P_{out} = P_{out}(t) - P_{out}(t_{0-})$ are valid as well. The contributions $\Delta Q_e, \Delta P_{in}, \Delta P_{out}$ change very slowly compared to ΔW_e and a good approximation of (13) in many cases is the assumption for continuity of their response, i.e. $\Delta Q_e, \Delta P_{in}, \Delta P_{out} \approx 0$. Then the total ECRH absorbed power can be determined directly from the changes of the total stored energy: $P_{ECRH} = d\Delta W_e/dt$. It should also be accounted for, however, that the assumption for continuity of the response of the heat flow and the total power of sources and sinks in some cases could be too strong. These contributions do not depend only explicitly on the T_e response to the additional heating power entering the plasma. The transport coefficients and the power densities of inputs and sinks might depend in an implicit way on the type of the additional heating power. This restricts the power balance schemes to be done in a much shorter time scale than the confinement time.

6   Experimental results

6.1   Results for total ECRH power

If the discharge is in steady state before applying the ECRH power then, (13) can be rewritten for the absolute values of the electron energy $W_e = \int_{V_s} 3/2 n_0 T_e dV$, the heat flow $Q_e = \oint_{S_s} q_e dS$ and the total power of sources P_{in} and sinks P_{out}:

$$P_{ECRH} = \frac{dW_e}{dt} + Q_e - P_{in} + P_{out} \tag{14}$$

According to (14) the power balance from ASTRA, using the experimental $T_e(\rho, t)$ profile evolution when ECRH is switched-on, gives P_{ECRH}. An experimental example for an Ohmic discharge at low density is shown in Figure 8. The power balance scheme in the shown example is performed by ASTRA which calculates numerically the change of the total stored energy P_w directly from the provided experimental T_e profile evolution. All other contributions are derived selfconsistently according to the smoothed T_e profile evolution which ASTRA yields so as to match the experimentally measured electron temperature. The jumps in P_{ECRH} and P_w evolution are not real but mark the slices for which the calculation was performed based on the experimental temperature profiles. The ECRH power was switched on at $t_0 = 2.000s$ and, as Figure 8 shows, $10ms$ after that the largest contribution in the energy balance comes from the
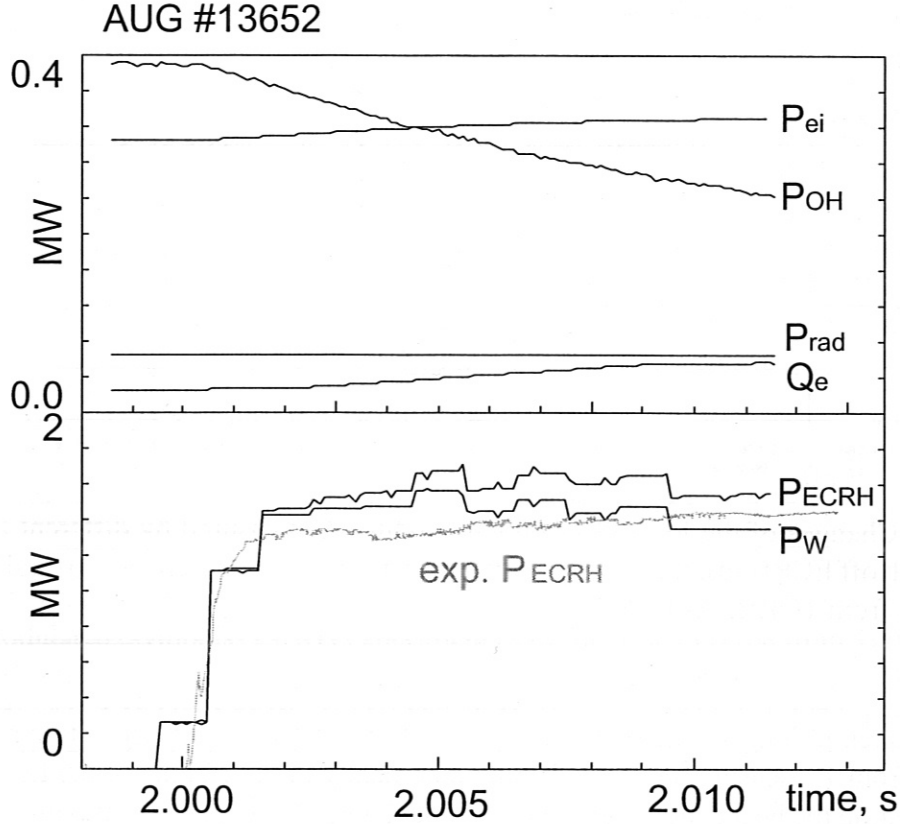
15

Figure 8: Power balance at switch on ECRH power yielding P_{ECRH} compared to the launched P_{ECRH} experimentally measured by the detectors (grey curve). In the power balance scheme the following contributions are accounted for: the change of the total stored energy $P_w = dW_e/dt$, the Ohmic heating power P_{OH}, the losses due to the energy exchange between electrons and ions P_{ei} and radiation P_{rad} and the total heat flow through the plasma boundary Q_e.

$P_w = dW_e/dt$ term. The calculated Ohmic heating P_{OH} in this time interval drops by $\approx 30\%$. The two main sinks are the energy exchange between electrons and ions, P_{ei}, and the radiative power P_{rad} and the former one slightly increases with T_e. The total heat flow through the plasma boundary Q_e also increases by $\approx 100\%$ but its contribution is still negligible. As it can be seen from the figure the assumption $P_{ECRH} = dW_e/dt$ is acceptable for the very first $2ms$ after switching on ECRH and the obtained P_{ECRH} in this case is $\approx 1.46MW$. At $t \approx 2.002s$ the unbalanced contributions P_{in} and P_{out} start to play role in (14) pointing out that in long time interval they should be accounted for in the used approach. The ECRH power derived after averaging over the plateau between $2.002s$ and $2.012s$ is $\approx 1.6MW$ and that coincides well with the applied one, shown by a grey curve in Figure 8, which is measured by the detector in the transmission line with accuracy of about 10%.

6.2   Results for the ECRH deposition center

As it was discussed in Sec.5 the use of equation (12) for the full reconstruction of $p_{ECRH}(\rho)$ in **switch on/off ECRH** experiments is limited by the quick broadening caused of the measured T_e profiles.

Even if the width of the deposition profile is difficult to be recovered if the temperature varia-
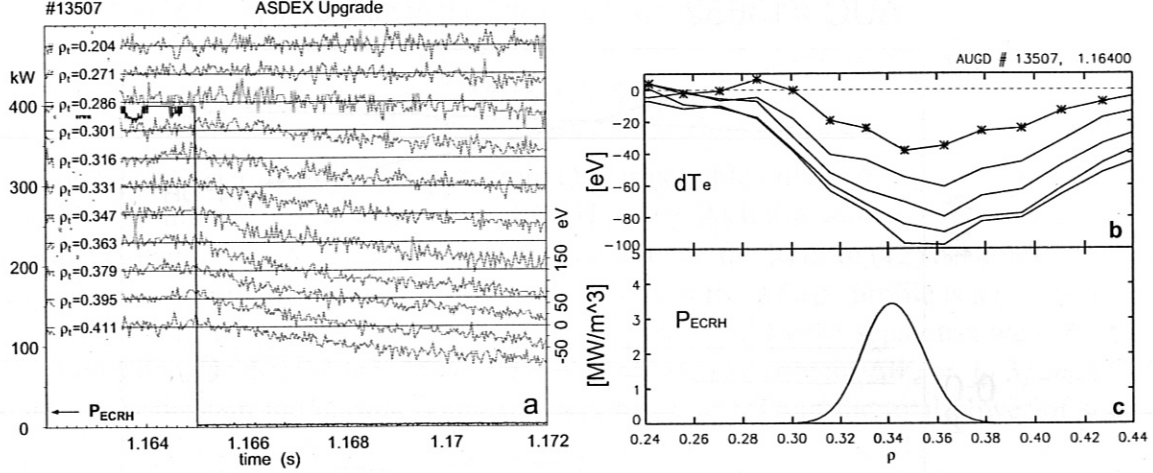
Figure 9: Changes of the local electron temperature T_e measured by different ECE channels after switch off ECRH (a), the corresponding $dT_e(\rho)$ profile with step $1ms$ (b) and ECRH power deposition from TORBEAM (c)

tions are taken in longer time scale, the center of the ECRH power deposition still can be determined from T_e measurements. Assuming that locally in the vicinity of the ECRH power deposition region the heat conductivity χ_e does not change drastically, the maximum of dT_e when ECRH is switched off should correspond to the maximum of the ECRH power deposition. An example is shown in Figure 9. The maximum of $dT_e(\rho)$ can also be observed visually if ECE channels are plotted together with the changed ECRH power, Figure 9a. The comparison of the $dT_e(\rho)$ profile and the calculated $p_{ECRH}(\rho)$, see Figure 9b and Figure 9c, confirms the conclusions drawn in Sec.5 that the maximum of the $dT_e(\rho)$ profile in the described time range of $5ms$ always indicates the deposition center and that the $dT_e(\rho)$ profile $1ms$ after switch off, the curve marked with asterisk in Figure 9b, is already quite broad compared with $p_{ECRH}(\rho)$, Figure 9c. Experimental deposition centers ρ_{pol0}, when launching ECRH perpendicularly, i.e. $\varphi = 0°$, for different poloidal angles θ, derived from the maximum change of T_e after switching off/on ECRH are plotted by bars in Figure 10 as a function of ρ_{pol0} from TORBEAM for the corresponding shot. Each bar in Figure 10 covers the region between the two adjacent ECE channels with the greatest dT_e. Hence the bars are bigger if these ECE channels are further apart. These experimental results from switched off/on ECRH studies taken from different discharges amongst ECRH shots in ASDEX Upgrade show good agreement with the positions obtained from beamtracing. The evaluation of switch on/off events may be strongly disturbed by sawteeth and for that reason not all the ECRH shots are useful.

The deposition centers can be more precisely derived from the maximum of $\tilde{T}_e$ profile in **modulated ECRH** experiments. Now the problems arising from the need to avoid sawteeth in switch on/off ECRH experiments are reduced. By applying FFT the sawteeth can generally be filtered out and ρ_0 can be more precisely determined. Number of shots in ASDEX Upgrade with fixed magnetic field, equilibrium and plasma parameters and different launching angles were performed with modulated ECRH. In the case of perpendicular launching the results for three different magnetic fields and at low density $n_0 \approx 2 - 4.5 \times 10^{19} m^{-3}$ are shown by symbols in Figure 10. Good agreement between the experimental and calculated deposition centers is observed in the three cases of perpendicularly launched EC beam even when the beam is diverged much from the magnetic axis. In the case of oblique launching, $\varphi \neq 0°$, and off-axis with $\theta = -25°$ the largest discrepancy between the derived and calculated ρ_{pol0} is observed at $\varphi = 27°$. It could
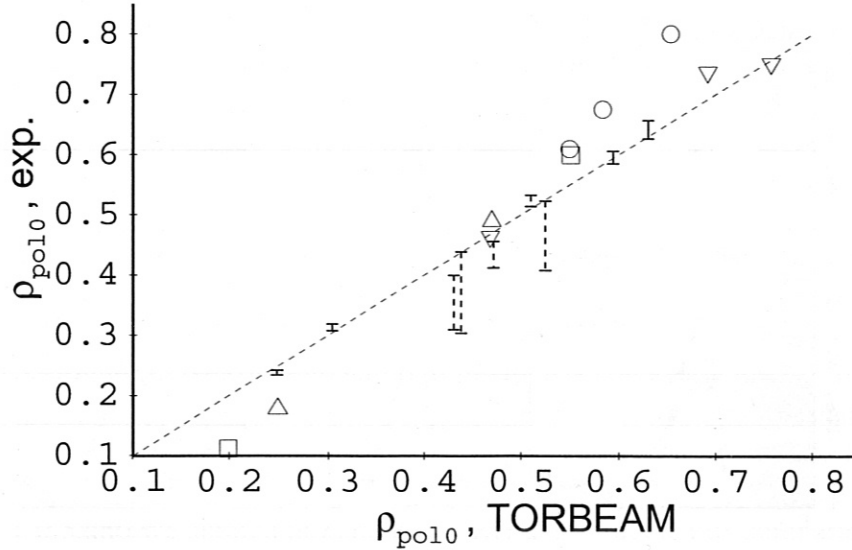
Figure 10: ECRH deposition centers from maximum change of T_e in switch-on (—), switch-off (- - -) and modulated (symbols) ECRH experiments as a function of ρ_{pol0} from TORBEAM. In modulated ECRH experiments the symbols are as follow: perpendicularly, $\varphi = 0°$, launched EC beam at $B_t = -2.15T(\triangledown)$, at $B_t = -2.32T(\square)$, at $B_t = -2.52T(\triangle)$ and obliquely launched off-axis, $\varphi \neq 0°$, $\theta = -25°$, EC beam at $B_t = -2.36T(\circ)$.

be due to errors arising from uncertainties in magnetic field B or plasma density n. The central plasma density in this case was $n_0 \approx 4.5 \times 10^{19}m^{-3}$ i.e. diffraction of the beam becomes effective. Consequently, small discrepancies in B, n or in the direction of the launched beam, angles θ and φ, produce large uncertainties in ρ_{pol0} determination.

6.3 Estimation of ECRH deposition width

The determination of the width w_0 of the ECRH power deposition profile $p_{ECRH}(\rho)$ is the most difficult from experimental point of view. As it was mentioned, the perpendicular diffusion will change $\delta T_e(\rho, t)$ in the finite time for which the electron energy will be distributed around the flux surfaces thus we always will measure a $\delta T_e(\rho)$ profile broader than the calculated $p_{ECRH}(\rho)$ profile. The estimates presented in Sec. 5.1 also show that very narrow ECRH deposition profiles, e.g. $w_0 \lesssim 0.01m$, cannot be recovered from T_e measurements. In both cases of switch on/off and modulated ECRH the critical parameter in w_0 determination is the characteristic time a. Since it is difficult to measure dT_e for times $t_{meas} < a \lesssim 200\mu s$ or $\tilde{T}_e$ for high enough frequencies $f_m > 1/(2\pi a)$, we estimate the ECRH deposition width w_0 in an indirect way, in which $dT_e(\rho)$ or $\tilde{T}_e(\rho)$ profiles determined experimentally after subtraction or from FFT are compared to those calculated by ASTRA. The deposition width w_0 in ASTRA is varied and the best match between the calculated and experimentally derived $dT_e(\rho)$ or $\tilde{T}_e(\rho)$ profiles should indicate the realistic value of w_0. The comparison of $dT_e(\rho)$ time evolution or equivalently of $\tilde{T}_e(\rho)$ dependence on f_m with the experimental results should confirm that value of w_0.

In the **switch on/off ECRH** studies T_e is taken experimentally in the steady state phase before changing ECRH source while the density n_e is fixed and supposed to be unchanged with ECRH. In ASTRA calculations the center of the ECRH power deposition ρ_0 is set as given from TOR-BEAM or slightly shifted around this value so to have the best agreement with the experimental $dT_e(\rho)$ profile. In Figure 11 the calculated $dT_e(\rho)$ profiles $2ms$ and $3ms$ after switching on ECRH
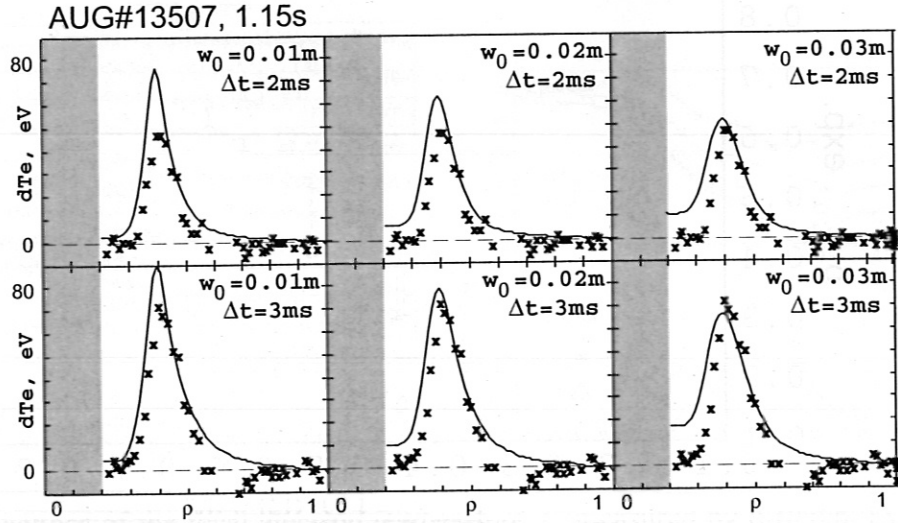
18

AUG#13507, 1.15s

Figure 11: Comparison of the experimentally derived (*) and calculated (—) temperature jump $dT_e(\rho)$ 2ms and 3ms after switching on ECRH power for different values of w_0

power for three values of w_0 are compared with the experimental data. This experiment was performed at low density $n_{e0} = 4 \times 10^{19}m^{-3}$, at $B_t = -2.5T$ and the beam was launched perpendicularly, $\varphi = 0°$, and off-axis, $\theta = -25°$. The very inner part of $dT_e(\rho)$ profile, i.e. at $\rho < 0.2$ is excluded from considerations because of strong sawteeth activity there. From Figure 11 it can be concluded that $dT_e(\rho)$ profiles from ASTRA do not match well the experimental profiles for the broadest $p_{ECRH}(\rho)$ profile, i.e. at $w_0 = 0.03m$. In this case the $dT_e(\rho)$ profile as derived from ASTRA is broader and its maximum increases slower than the experimental one although they coincide at $\Delta t = 2ms$. The narrowest $p_{ECRH}(\rho)$ profile, i.e. at $w_0 = 0.01m$ matches very well the inner and outer branches of $dT_e(\rho)$ profile but the calculated $dT_e(\rho)$ maximum in this case is larger than the experimental one. Figure 12 shows the switch off for the same pulse and
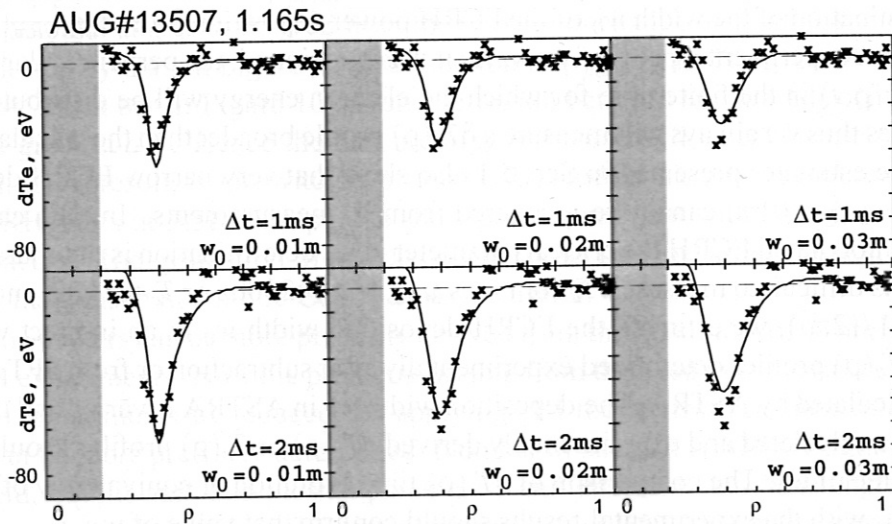
AUG#13507, 1.165s

Figure 12: Comparison of the experimentally derived (*) and calculated (—) temperature drop $dT_e(\rho)$ 1ms and 2ms after switching off ECRH power for different values of w_0

here we can see that the broadest $p_{ECRH}(\rho)$ profile could be ultimately excluded. In the switch

19

off case the best match between the calculated and the experimental $dT_e(\rho)$ profiles is observed at $w_0 = 0.01m$. Comparing switch on and switch off, Figures 11 and 12, we conclude that w_0 is in the range $0.01m < w_0 < 0.02m$. In this case according to TORBEAM the power deposition profile width is $w_{TB} = 0.013m$.

The ECRH deposition width can also be determined by using FFT analysis of the temperature perturbations $\tilde{T}_e$ in **modulated ECRH** experiments. The propagation of the heat pulses induced by modulated ECRH is characterised by the heat pulse diffusivity $\chi_e^{HP} \equiv \chi_{e,eff}$ which describes the diffusive broadening of $\tilde{T}_e(\rho)$ profile and in general is larger than power balance diffusivity χ_e [26, 27]. As explained in Sec. 5.1, (equation (11) and Figure 7) the heat pulse diffusivity χ_e^{HP} strongly contributes to the apparent width of the ECRH deposition profile. In our study we confirm this expectation experimentally. That was done in two identical discharges, one with low and the other with high χ_e^{HP} following the observations described in [22]. In the first one we applied off-axis cw ECRH $(0.8MW)$ at $\rho = 0.58$ leading to reduced transport in the central region, $\rho < 0.5$ and we applied modulated ECRH at $\rho = 0.45$. For comparison in the second experiment we applied on-axis cw ECRH $(0.8MW)$ at $\rho = 0.24$ which increases χ_e^{HP} in the $\rho > 0.3$ region. The modulated ECRH was placed at the same place as in the first experiment but now the heat pulse diffusivity χ_e^{HP} in this region is larger. The importance of lower trans-
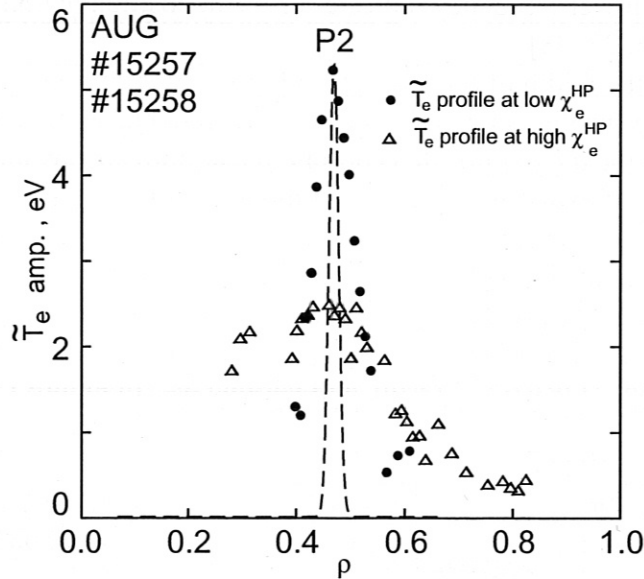

Figure 13: $\tilde{T}_e(\rho)$ profiles experimentally derived by FFT of T_e in the cases of reduced and enhanced transport compared with $p_{ECRH}(\rho)$ from TORBEAM (- - -).

port to get $\tilde{T}_e(\rho)$ profile closer to $p_{ECRH}(\rho)$ is clearly seen when the experimental $\tilde{T}_e(\rho)$ profiles, obtained from FFT, are compared, Figure 13. The distinct broadening of $\tilde{T}_e(\rho)$ and decreasing of its amplitude with increasing χ_e^{HP} is as expected from equation (11) and Figure 7 and these experimental results further point out the scenario shown in Figure 14a as the most suitable in w_0 estimations. The narrowing of $\tilde{T}_e(\rho)$ profile with f_m is also observed but as the results and the calculations show even when $f_m = 1kHz$ the profile $\tilde{T}_e(\rho)$ is still broader than the calculated ECRH power deposition profile. The change of χ_e^{HP} in on-axis and off-axis ECRH experiments is investigated also by ASTRA simulations. The results for T_e, χ_e and χ_e^{HP}, derived from (5), from these simulations are shown in Figure 14. Within the transport model [25] used in AS-TRA, χ_e^{HP} decreases by about 1.3 to 5 times in off-axis cw ECRH experiment compared to the on-axis cw ECRH experiment. The analysis of the heat pulse propagation in similar experi-
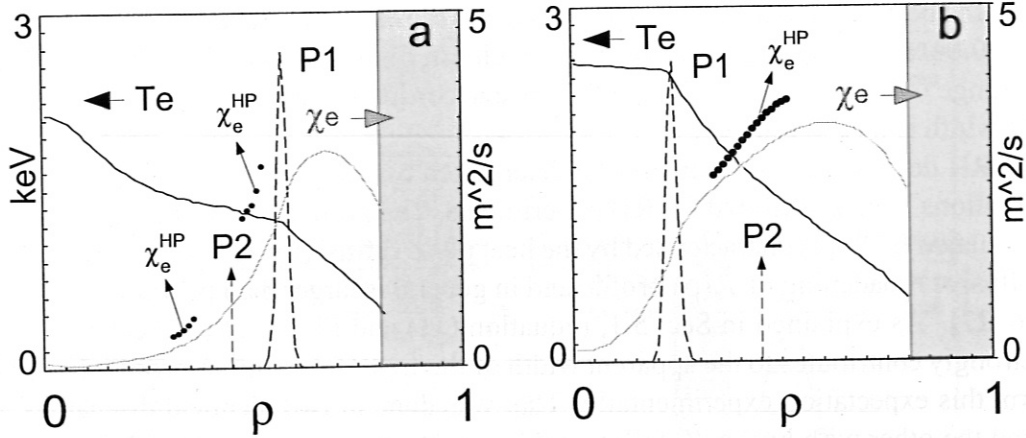
Figure 14: ASTRA simulations of the experiments with reduced transport in the inner (a) from the cw ECRH P1 deposition region and enhanced transport in the outer region (b). The modulated $f_m = 500Hz$ second ECRH P2 deposits in both regions.

ments performed at lower frequency indicate for the deposition region an increase of χ_e^{HP} by a factor of about 5 [26, 27, 28].

The comparison of the width of the $\tilde{T}_e(\rho)$ profile for different frequencies is analogous to the comparison of $dT_e(\rho)$ profile time evolution. Higher frequencies f_m correspond to smaller time interval Δt in which the $dT_e(\rho)$ profile is observed and both are advantageous in $p_{ECRH}(\rho)$ approach. A sequence of experiments [29] with modulated ECRH at different frequencies $f_m = 30Hz - 2kHz$ was performed in ASDEX Upgrade in a similar way as shown in Figure 14a. The goal of these experiments is to obtain an estimate of w_0 by determining the central amplitude and the width of the $\tilde{T}_e(\rho)$ profile at different frequencies f_m similarly to Figure 7. The $\tilde{T}_e(\rho)$ profiles are calculated with ASTRA taking ρ_0 as derived from FFT of the experimental data, slightly different from TORBEAM result, and varying w_0. In Figure 15 three $\tilde{T}_e(\rho)$ profiles for
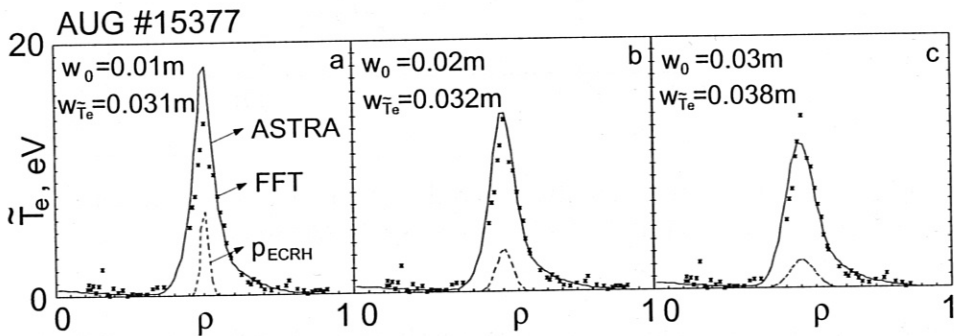
Figure 15: Experimental $\tilde{T}_e(\rho)$ profiles from FFT (*) and from ASTRA (—) for three different values of w_0 and $f_m = 300Hz$. Dash lines show the deposition profile from TORBEAM and $w_{\tilde{T}_e}$ is the estimated width of the corresponding $\tilde{T}_e$ profile.

three different values of w_0 are shown and compared with the experimental results from FFT. The best match in Figure 15 is observed for $w_0 = 0.02m$. The TORBEAM result for these experimental conditions was $w_0 \approx 0.01m$ and as Figure 15a shows this would result in a narrower and more peaked $\tilde{T}_e(\rho)$ profile. Figure 15 also shows that the frequency $f_m = 300Hz$ is too low to yield directly $p_{ECRH}(\rho)$.

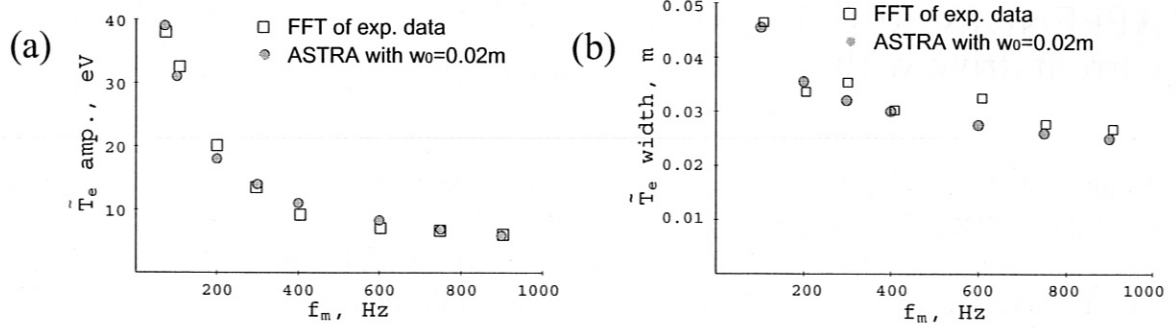Figure 16: $\tilde{T}_e$ amplitudes (a) and widths (b) from ASTRA and FFT for $w_0 = 0.02m$

The value $w_0 = 0.02m$ was then used to analyze the frequency scan, whose results are shown in Figure 16. The experimental and calculated amplitudes agree well, Figure 16a. They clearly follow the expected behaviour and decrease strongly with f_m as predicted from the slab model. The experimental widths, Figure 16b, are derived by linear interpolation of FFT data from ECE and they coincide rather well with the data simulated by ASTRA.

The estimated value of the ECRH deposition width $w_0 = 0.02m$ is twice larger than the width given by the TORBEAM code. As it was mentioned in Sec. 4 TORBEAM calculates the "pure" $p_{ECRH}(\rho)$ which is the EC absorption profile, as it occurs along the beam path, after mapping onto the flux surfaces. On the other hand we measure the ECRH deposition profile from the T_e response and this suggests that the transport effects are involved into the experimental determination of $p_{ECRH}(\rho)$. Both the calculated "pure" $p_{ECRH}(\rho)$ and the measured ECRH deposition profile are identical only if the absorbed heat distributes instantaneously over the flux surfaces and the T_e response is measured in a shorter time scale compared to the characteristic time a, i.e. $t_{meas} < a$. As far as these two conditions are not fulfilled in our study we always will estimate experimentally some broader ECRH deposition profile than the calculated $p_{ECRH}(\rho)$. Actually we cannot predict exactly how much broader the measured ECRH deposition profile is compared to the calculated one. The solutions from the slab model and the estimates in Sec. 5.1 show that for the typical cases we can expect that we measure ≈ 1.5 times broader profile. Another source of discrepancies between the calculated and the measured ECRH power deposition width are the input beam parameters. For instance, the initial beam width, which influences directly the calculated $p_{ECRH}(\rho)$, is not measured experimentally but calculated.

APPENDIX A: Calculation of ECRH power deposition and EC current drive with `torbeam` and `xbt` graphical interface

An integrated tool for calculation and presentation of the beamtracing results is developed and utilized in ASDEX Upgrade. It consists of the following modules:

(*i*) `xbt` — graphical interface, Figure 17, that facilitates the setting and the alteration of the input parameters for the beamtracing calculations and for the plot of the results;
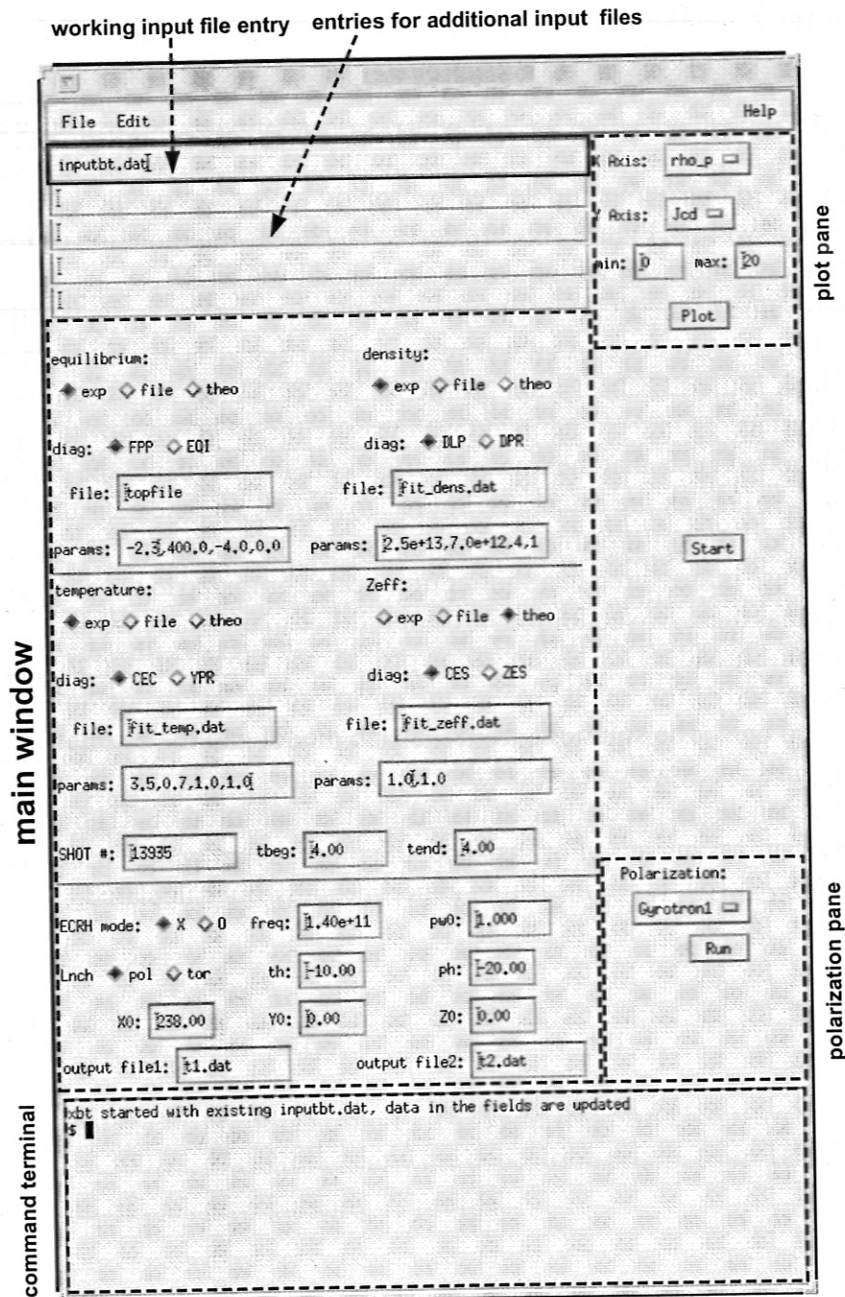
(*ii*) `torbeam` — the beamtracing code;

Figure 17: The `xbt` graphical interface

(*iii*) `plotsrv` — a programme that plots the results from the beamtracing calculations, e.g.

beam path, ECRH power deposition $p_{ECRH}(\rho)$ and ECCD $j_{ECCD}(\rho)$ profiles, etc.;

(*iv*) `plotprf` – an auxiliary programme plotting n and T_e profiles and providing additional information which is essential for the beamtracing calculations;

(*v*) `polar` – a programme that calculates angles for the polarization mirrors.

All modules interact with each other by input file, in which all the important settings are saved. Further we will refer to this input file as *inputbt*[2]. In the following all the modules will be explained separately in detail.

Module `xbt`

`xbt` is the main programme which interacts with the other modules and provides user friendly interface. It can be started by typing `/u/kvk/1/xbt&` from the command line of usual SUN workstation working with `SunOS` or by typing `/u/kvk/1/solaris/xbt&` from the command line of a workstation working with `Solaris`.

The file name listed in the working input file entry of `xbt`, Figure 17, is the working *inputbt* file. All other fields in `xbt` main window, Figure 17, are set up according to the settings in that file. Changing the file name in the working input file entry to a name of another existing *inputbt* file automatically updates the setting in the main window according to the new *inputbt*. From the other side every push of *Plot* or *Start* button saves the settings listed in the `xbt` main window in the actual working *inputbt* file. When starting `xbt` if a file named *inputbt.dat* does not exist it is created automatically with the default settings which are also displayed in the `xbt` main window. If *inputbt.dat* already exists, for instance from some other previous `xbt` run, then every new `xbt` start will read the settings from that file and the fields in the `xbt` main window will be updated according to the content of that *inputbt.dat* file. Up to four additional *inputbt* files can be set in the provided four entries for additional input files, situated below the working input file entry, Figure 17. These additional *inputbt* files are not utilized for beamtracing calculations but are used only by the plotting modules `plotsrv` and `plotprf`. In such a way one is able to plot and compare up to five different beamtracing outcomes or experimental conditions.

The fields in `xbt` main window have the following meaning. The top field is separated in four subdivisions: *equilibrium, density, temperature* and *Zeff*. They have similar structure and present an option for choosing the type of the data: *exp* for experimental data, *file* for data from file and *theo* for analytically expressed quantities. When experimental data are desired the name of the corresponding AUG diagnostic should be selected from the choice *diag*. The diagnostic options at the present moment are: *FPP* and *EQI*[3] for the equilibrium, *DLP* and *DPR* for the density, *CEC* and *YPR* for the temperature. If the required data for a given shot cannot be yielded by any of the presented diagnostics then the torbeam calculations can be provided with data from file which substitutes the missing diagnostic. This can be done by selection the *file* option and setting the proper file name in the *file* text field. The file *topfile* is created automatically when `torbeam` with experimental equilibrium is started and can be used when one performs second run of the code with the same equilibrium. In case of missing density or temperature profiles or necessity for smoothed data one could select the *file* option for density or temperature and start beamtracing with data from file. The files[4] *fit_dens.dat* and *fit_temp.dat* should be ASCII format with two columns and 101 rows. In the first column one should supply ρ_p from $\rho_p = 0$ to $\rho_p = 1.0$ with step 0.01 and in the second one the corresponding density in cm^{-3} for *fit_dens.dat* or electron temperature in *keV* for *fit_temp.dat*. It is also possible to perform torbeam calculations with analytical equilibrium and kinetic profiles. That can be done by choosing the *theo*

---

[2]Of course it can have arbitrary valid name

[3]this diagnostic is not yet fully supported by `torbeam`

[4]As *inputbt* file they can have arbitrary valid name

option and setting the right parameters in *params* text field. The parameters for the equilibrium include eight quantities, ordered as follows: $B_t, I_p, \Delta_0, \Delta_e, \kappa_0, \kappa_e, q_0, q_e$ The first four of them specify the toroidal magnetic field B_t in T, the plasma current I_p in kA and the Shafranov shift in the center Δ_0 and at the edge Δ_e in cm so that its profile will be $\Delta(\rho) = \Delta_0 + (\Delta_e - \Delta_0)\rho^2$. The other four parameters determine the elongation and the safety factor profiles according to $\kappa(\rho) = \kappa_0 + (\kappa_e - \kappa_0)\rho^2$ and $q(\rho) = q_0 + (q_e - q_0)\rho^2$, where q_0 and q_e are the safety factor in the center and at the edge and ρ is the flux surface label. Note that `torbeam` calculation with analytical equilibrium cannot be processed and displayed by the plotting modules `plotsrv` and `plotprf`. If analytical density and temperature profiles are selected by choosing *theo* option for them then the following parameters should be set in the corresponding *params* text fields. The density parameters are $n_0, n_{edg}, e1, e2$ where n_0 and n_{edg} account for the density in cm^{-3} in the center and at the edge and so the density profile will be expressed analytically as $n(\rho_p) = (n_0 - n_{edg}) * (1 - \rho_p^{e1})^{e2} + n_{edg}$. The same is valid for the temperature parameters $T_{e0}, T_{eedg}, te1, te2$ where T_{e0} and T_{eedg} are the electron temperature in keV in the center and at the edge and the temperature profile will be: $T_e(\rho_p) = (T_{e0} - T_{eedg}) * (1 - \rho_p^{te1})^{te2} + T_{eedg}$. The analytical Z_{eff} is supposed to have parabolic profile according to $Z_{eff}(\rho_p) = Z_{eff0} + (Z_{effedg} - Z_{eff0})\rho_p^2$ where Z_{eff0} and Z_{effedg} should be given in the *params* text box belonging to *Zeff* field. In such a way giving equal values to Z_{eff0} and Z_{effedg} means flat Z_{eff} profile.

Further in the `xbt` main window in the fields *SHOT #* and *tbeg* the corresponding shot number and the shot time should be set. If the value in *tend* is different from that in *tbeg* the experimental $n(\rho)$ and $T_e(\rho)$ profiles will be averaged in the indicated time interval, i.e. from *tbeg* to *tend*. The next field in the `xbt` main window is the field for setting ECRH parameters. The mode, the frequency and the power of the launched ECRH could be set in the corresponding fields, i.e. *ECRH mode, freq* and *pw0*. The poloidal launching angle θ of the beam can be set in the *th* field, and the toroidal launching angle φ can be adjusted in the *ph* field. Setting *th* to negative values means we are deviating the beam up from the torus midplane, so that $\theta \approx -10°$ is on-axis beam. If the toroidal launching angle in the *ph* field is set to be less than zero we will produce negative EC current drive, or this corresponds to ctr-CD scenario. The fields *X0, Y0* and *Z0* account for the initial position of the launched beam. In ASDEX Upgrade these settings should be: *X0*= 238.00 cm, *Y0*= 0 cm and *Z0*= 0 cm for gyrotron 1 and 2 and *X0*= 231.10 cm, *Y0*= 0 cm and *Z0*= 0 cm for gyrotron 3 and 4. These fields are also updated automatically when the corresponding gyrotron is chosen from the polarization pane. The last fields are *output file1* and *output file2*. They specify the names of the output files in which `torbeam` saves its results. These files should be unique and different for different *inputbt* files.

When all the settings are done one can start `torbeam` by pressing the *Start* button. That will save all the parameters into the actual working *inputbt* file and will proceed this file to `torbeam`. When the *Plot* button is pressed depending on the chosen *Y Axis* in the plot pane, Figure 17, beamtracing results or kinetic profiles will be plotted by the programmes `plotsrv` or `plotprf`. If one intends to plot the beamtracing results with `plotsrv` first he should ensure that the output files in the fields *output file1* and *output file2* exist and then to set *Y Axis* to *Jcd* or *Pde*. If *Y Axis* is set to *ne* or *Te* the density and the temperature profiles will be plotted by `plotprf` and additional information related to the calculations will be reported. The number set in the *max* field will determine the scale for plotting the quantity shown in *Y Axis*. By the option *X Axis* one can change the horizontal axis of the plot to be ρ_p or ρ_t.

Module `plotsrv`
The `plotsrv` module is the main plotting tool which displays the results from beamtracing. It also reports an useful information about ECRH power deposition profile $p_{ECRH}(\rho)$, the ECCD

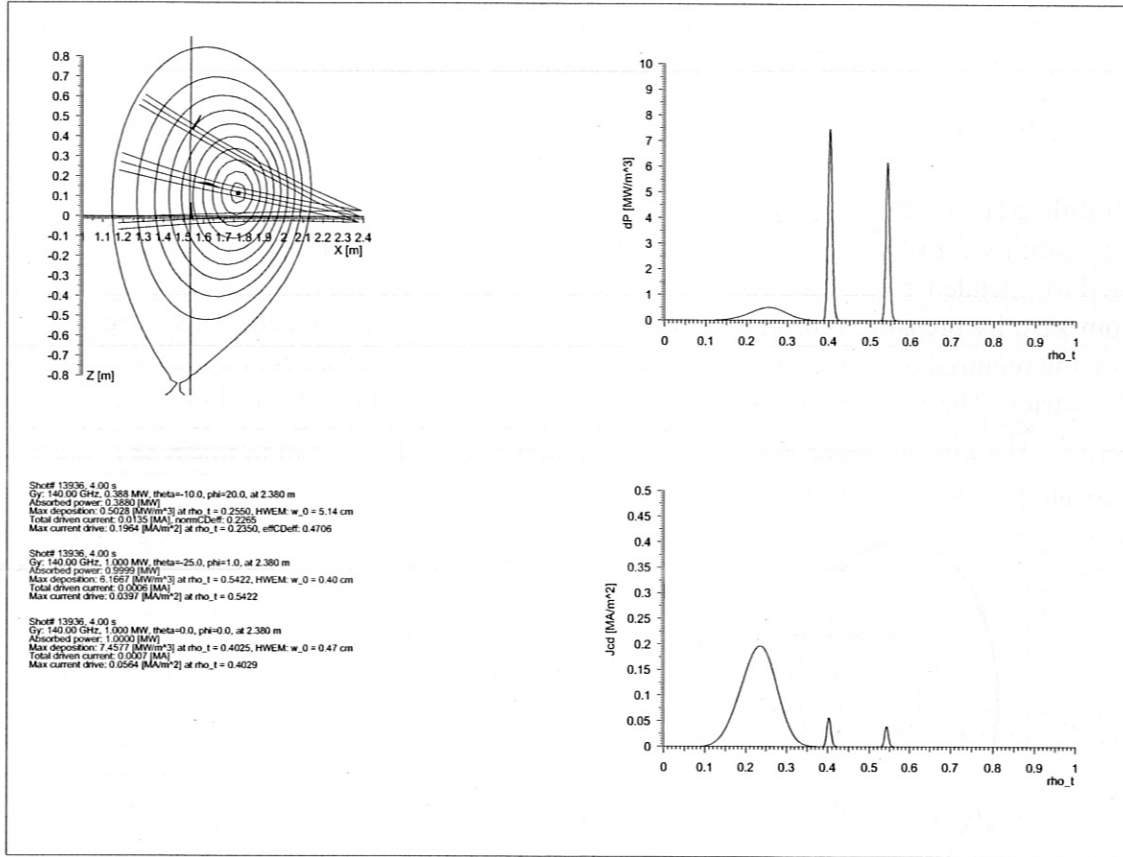density profile $j_{ECCD}(\rho)$ and CD efficiency, Figure 18. The `plotsrv` programme uses the

Figure 18: The plot of the `torbeam` results by `plotsrv`

`pplot` packet and can also be started separately from the command line. Up to 5 different profiles can be processed and displayed by `plotsrv`. It draws the beam path in the plasma cross-section together with the $\rho_p = 0.0, 0.1, ..., 1.0$ surfaces. For the working *inputbt* file the classical resonance layer is displayed as well. `plotsrv` plots also the ECRH power deposition profile $p_{ECRH}(\rho)$ and ECCD density profile $j_{ECCD}(\rho)$ and ρ could be either normalized poloidal flux radius or normalized toroidal flux radius depending on the selected *X Axis* in `xbt`. The report displays the shot number and shot time for the selected experimental equilibrium, the frequency of the EC beam, the initial power, the launching angles and the initial position of the beam. All these are quantities according to which the presented results are derived. The information about the ECRH power deposition profile $p_{ECRH}(\rho)$ includes its maximum $p_{ECRHmax}$, its half width w_0, determined at $p_{ECRHmax}/e$, the total absorbed ECRH power P_{ECRH} and the deposition center ρ_0. Concerning the ECCD the following quantities are determined and included in the `plotsrv` report: the total driven current I_{ECRH}, the maximum $j_{ECCDmax}$ of EC current drive profile and its center. If the *inputbt* file for the last `torbeam` run is presented in the `xbt` working input file entry before starting `plotsrv` then ECCD efficiencies for this calculation will be reported as well. The normalized ECCD efficiency appears as *normCDeff* in the report and is defined [7] as:

$$\zeta_{EC} = 3.27\frac{I_{EC}[MA]n[10^{19}m^{-3}]R[m]}{P_{ECRH}[MW]T_e[keV]}, \tag{15}$$

where n is the electron density, T_e is the electron temperature and R is the plasma major radius.

The ECCD efficiency calculated according to:

$$\eta_{EC} = \frac{j_{ECRHmax}[MAm^{-2}]n(\rho_0)[10^{19}m^{-3}]}{P_{ECRHmax}[MWm^{-3}]T_e(\rho_0)[keV]},$$
(16)

is noted by *effCDeff* and is used in ASTRA calculations.

Module `plotprf`

A possibility for plotting the plasma shape, n and T_e profiles and displaying an information related to intended `torbeam` calculations is provided by `plotprf` module. It can be started from `xbt` by pressing *Plot* button while *ne* or *Te* in *Y Axis* is chosen. This programme deals with the required quantities according to the settings, found in the *inputbt* files listed in the `xbt` file entries. The `plotprf` tool uses the `pplot` packet and one typical plot is shown in Figure 19. The plasma shape for the selected experimental equilibrium is displayed by drawing
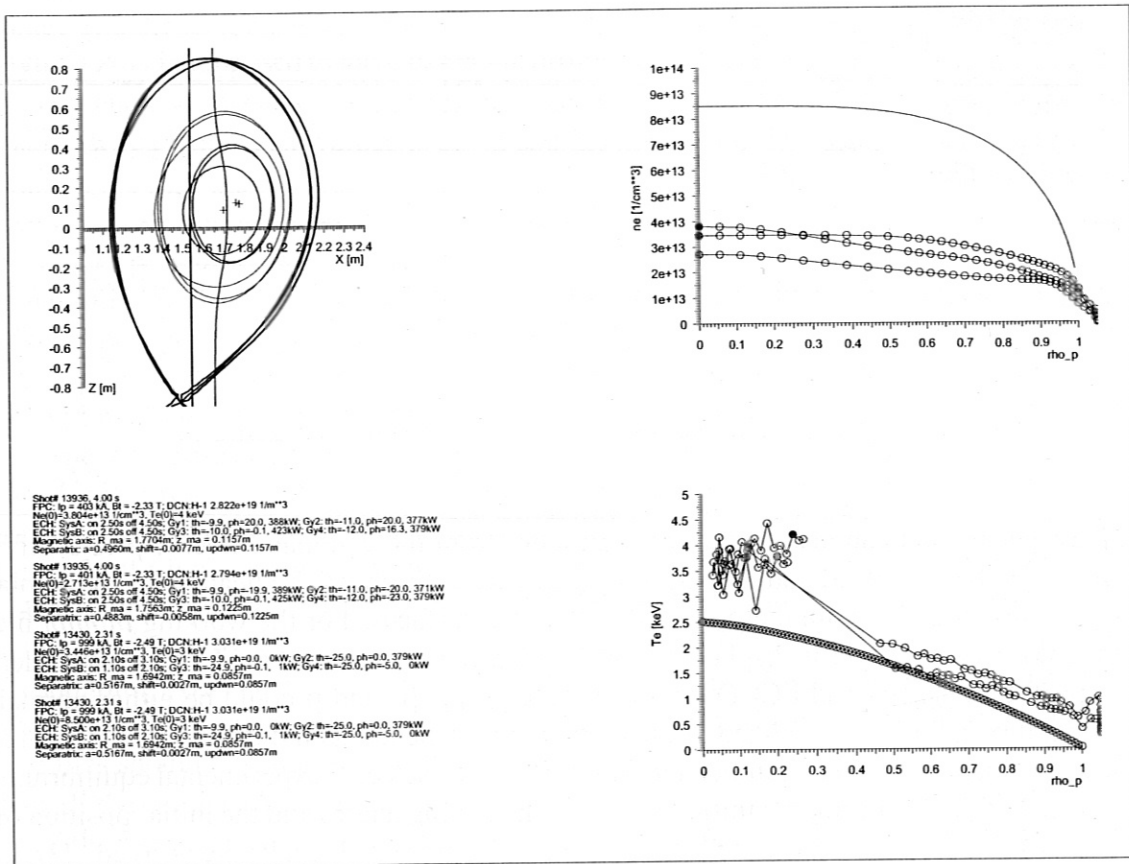

Figure 19: The plot of the `torbeam` settings by `plotprf`

the separatrix, magnetic axis and $\rho_p = 0.5, 0.75$ surfaces. Details about the separtrix and the magnetic axis can be found in the report field as well. For the frequency shown in the *freq* field of `xbt` the classical resonance layer for the 2nd harmonic EC beam is displayed and that helps one to envisage the eventual position of the EC absorption. The density and the electron temperature profiles are plotted as they will be accepted by `torbeam`, i.e. from experiment, from file or analytically expressed ones. In the report some useful quantities are included and these are the toroidal magnetic field, plasma current, line averaged density, central density and temperature. A practical information concerning the gyrotron operation for the selected shot can be

found further in the report. The switching on and switching off times for System A (Gyrotron 1 and 2) and for System B (Gyrotron 3 and 4) are shown together with the launching angles for the corresponding gyrotrons. Here *th* and *ph* show the actual poloidal and toroidal launching angles. The launched power is taken for the indicated shot exactly at the moment displayed by *tbeg*.

Module `polar`

The programme `polar` calculates the polarization angles for the gyrotrons. It takes into account some settings from the `xbt` main window. The toroidal magnetic field B_t and the plasma current I_p are taken as they are set in the *params* text field belonging to *equilibrium*. The EC mode is determined according to the setting in *ECRH mode* and the launching angles are taken as they are indicated in *th* and *ph* boxes. Then after selection of the gyrotron number from the `xbt` polarization pane, Figure 17, and pressing the button *Run* the calculations with `polar` will be started. The result of the calculations is displayed on the `xbt` command terminal, Figure 17, and the information which is included in the that report consists of the angles of the polarization mirrors and specification of the poloidal ant toroidal angles as they should be accounted for in the ECRH control room.

Example 1: Calculation of the ECRH deposition profile and ECCD

A possible start of `xbt`, performing beamtracing calculations and plotting of the results could be done following these steps:

1). Create directory for specific experiment or shot and start `xbt` from that directory by typing `/u/kvk/1/xbt&`;

2). The *inputbt.dat* file with the default settings will be created automatically and these settings will appear in the `xbt` main window;

3). Choose *SHOT #*, *tbeg*, experimental equilibrium and the type of data you wish to provide to the code. The density and the temperature could be experimental, analytical or from file supposing the correct file is provided. From the choice *Y Axis* select *ne* or *Te* and press the *Plot* button. Then the `xbt` module will draw the plasma shape for the chosen shot and time and will plot the density and the temperature profiles as they are set in the `xbt` main window;

4). If all profiles and needed quantities are displayed correctly, find in the comment the gyrotrons settings, the power of the EC beam and the launching angles, and update them in the `xbt` main window. The poloidal and the toroidal angles for Gyrotron 1 and Gyrotron 2 can be taken directly from the report and set in the corresponding `xbt` fields, while the the launching angles for Gyrotron 3 and Gyrotron 4 should be slightly changed. Set the names of desired output files in the *output file1* and *output file2* fields and start beamtracing by pressing the *Start* button. If the experimental density or the experimental temperature cannot be provided by the diagnostic try to express them analytically;

5). When the beamtracing calculation finishes the results can be plotted, by setting *Y Axis* to *Jcd* or *Pdp* and pressing the *Plot* button.

Example 2: Setting up $p_{ECRH}(\rho)$ and $j_{ECCD}(\rho)$ profiles in ASTRA

Here an example for inclusion of the results from a beamtracing calculation in the transport code ASTRA is given. The described procedure is applied only for version 5.2 of the ASTRA code. Let us assume that a calculation of the ECRH deposition profile and ECCD is already performed following the explanations in **Example 1** and the results are displayed by `plotsrv`, Figure 18.

The needed quantities are: the absorbed ECRH power, the center of the deposition, the width of the deposition profile and the CD efficiency. In the first `plotsrv` report shown in Figure 18 they are indicated as follows: *Absorbed power: 0.3880MW, Max. deposition: ... at rho_t = 0.2550, HWEM: w_0 = 5.14cm* and *effCDeff: 0.4706*. From `plotprf` output, Figure 19, one can check again the applied ECRH power for this shot and take the times when the gyrotrons were switched on and off. The following example shows how one can implement the beamtracing results in ASTRA.

```
!-------------------ECRH  ----------------------------
! #13936, Gyrotron1
! Gaussian profiles of ECRH heating and ECCD efficiency
! rho_t=0.255,  HWEM: w_0=0.0514 in m,  effCDeff: 0.47
!
CV1=AMETR(0.255*ROC)/ABC; CF4=0.0514/ABC; CF13=0.47;
FGAUSS(CV1,CF4,CAR10):;
!
! Power Gyrotron1 P_G1=388kW, cw
! switched on at 2.5s , switched off at 4.5s
CF15=0.388*(FJUMP(2.50)-FJUMP(4.50));
!
PEECR=CF15*CAR10;
CUECR=CF13*CF15*CAR10*TE/NE;
!-------------------ECRH  ---------------------------
```

By inclusion of these lines in the ASTRA model file one is able to simulate ECRH power deposition $p_{ECRH}(\rho)$ and ECCD $j_{ECCD}(\rho)$ taking the essential quantities from the output of `plotsrv`.

An useful information about `torbeam` and `xbt` could be found also on the web:
www.aug.ipp.mpg.de/~emp/btlinks/auginterf.html

References

[1] Leuterer F et al 2001 *AIP Conf. Proc. CP595* 259

[2] Hartfuss H et al 1986 *Nucl. Fusion* **26** 678

[3] Erckmann V, Gasparino U 1994 *Plasma Phys. Contr. Fusion* **36** 1869

[4] Erckmann V et al 1995 *Fusion Engineering and Design* **26** 141

[5] Rome M et al 1997 *Plasma Phys. Contr. Fusion* **39** 117

[6] Prater R et al 1998 *2nd Europhysics Topical Conf. on Radio Frequency Heating and Current Drive of Fusion Devices (Brussels, 1998)* **vol 22A** 221

[7] Petty C C et al 1999 *13th Topical Conf. on Radio Frequency Power in Plasmas (Annapolis, Maryland, 1999)* **AIP CP 485** 245

[8] Manini A et al 2002 *Plasma Phys. Contr. Fusion* **44** 139

[9] Cirant S et al 1994 *Proc. 15th Int. on Plasma Physics and Conf. on Controlled Nuclear Fusion Research* **vol 2** 159

[10] Cirant S et al 2002 *12th Joint Workshop on Electron Cyclotron Emission and Electron Cyclotron Resonance Heating (Aix-en-Provence, France, 2002)*

[11] Akulina D et al 2001 *Fusion Engineering and Design* **53** 321

[12] Leuterer F et al 1997 *Proc. 24th Eur. Conf. on Controlled Fusion and Plasma Physics (Berchtesgaden, 1997)*, **vol 21A** (Geneva: European Physical Society) part IV 1533

[13] Leuterer F et al 2001 *Fusion Engineering and Design* **56-57** 615

[14] Suttrop W et al 1996, Practical Limitations to Plasma Edge Electron Temperature Measurements by Radiometry of Electron Cyclotron Emission, Rep. IPP 1/306, Max-Planck-Institut für Plasmaphysik, Garching

[15] Schweinzer J et al 1995 *Proc. 22th Eur. Conf. on Controlled Fusion and Plasma Physics (Bournemouth, 1995)*, **vol 19C** (Geneva: European Physical Society) part III 253

[16] Poli E, Pereverzev G V, Peeters A G 1999 *Phys. Plasmas* **6** 5

[17] Poli E, Peeters A G, Pereverzev G V 2001 *Comput. Phys. Commun.* **136** 90

[18] Pereverzev G V 1998 *Phys. Plasmas* **5** 3529

[19] Westerhof E 1989, Implementation of Toray at JET, Rijnhuizen Report PR-89-183

[20] Jacchia A et al 1991 *Phys. Fluids B* **3** 3033

[21] Lopes Cardozo N J 1995 *Plasma Phys. Contr. Fusion* **37** 799

[22] Ryter F et al 2001 *Phys. Rev. Lett.* **86** 2325

[23] Tardini G et al 2002 *Nucl. Fusion* **42** L11

[24] Pereverzev G V et al 1991, ASTRA: An Automatic System for Transport Analysis in a Tokamak, Rep. IPP 5/42, Max-Planck-Institut für Plasmaphysik, Garching

[25] Nordman H et al 1990 *Nucl. Fusion* **30** 983

[26] Ryter F et al 2001 *Nucl. Fusion* **41** 537

[27] Ryter F et al 2001 *Phys. Rev. Lett.* **86** 5498

[28] Imbeaux F et al 2001 *Plasma Phys. Contr. Fusion* **43** 1503

[29] Leuterer F et al 2002 *12th Joint Workshop on Electron Cyclotron Emission and Electron Cyclotron Resonance Heating (Aix-en-Provence, France, 2002)*